Article to be submitted to Cement and Concrete Research

Alite-Belite-Ye'elimite cements: effect of dopants on the clinker phase composition and properties.

*Jesus D. Zea-Garcia[a], Isabel Santacruz[a], Miguel A.G. Aranda[a,b], Angeles G. De la Torre[a]**

[a] Departamento de Química Inorgánica, Cristalografía y Mineralogía, Universidad de Málaga, Málaga, 29071, Spain.

[b] ALBA Synchroton, Carrer de la Lum, 2-26, Cerdanyola, 08290, Barcelona-Spain.

* email: mgd@uma.es

KEYWORDS: clinkering, Ca_3SiO_5, $3CaO{\cdot}3Al_2O_3{\cdot}CaSO_4$, C_2S polymorphism, boron, fluor, zinc, alkaline oxides, X-Ray Diffraction & Rietveld method, EDS.

ABSTRACT: Clinkers with alite-belite-ye´elimite (ABY) are considered as eco-friendly cements. Clinkering (2 Kg) of two types of ABY clinkers was optimized: standard-ABY, with CaF_2 and ZnO as dopants (32.6 wt% alite, 30.4 wt% β-C_2S and 15.6 wt% ye'elimite) and αABY, with CaF_2, ZnO, B_2O_3, Na_2O (14.4 wt% alite, 37.1 wt% β-C_2S, 18.5 wt% α'_H-C_2S and 7.5 wt% ye'elimite). Zn and F were mainly incorporated in alite and ferrite as dopants determined by EDS semi-quantitative analysis. The effect of dopants on the hydration of the cement mortars has been tested. Thus, standard-ABY develops 29.9 MPa compressive strengths at 1 day while αABY does 16.8 MPa, mainly due to the higher amount of alite of the former. The presence of α'_H-C_2S in αABY increases mechanical strengths at 28 days of hydration from 44.7 MPa of standard-ABY to 74.9 MPa.

1. Introduction.

Portland Cement (PC) is the most used binder all over the world. However, during the manufacturing of one ton of PC, ~0.97 tons of CO_2 are released to the atmosphere, mainly due to the limestone calcination to achieve the desired composition [1]. As an example, during the formation of alite, C_3S, which is the main component of PC (> 65 wt%), 0.58 tons of CO_2 (per ton of alite) are released. Thus, the cement industry is responsible of ~6% of the anthropogenic CO_2 emissions [2]. An eco-friendly approach may consist on the design and fabrication of alternative cements, called eco-cements, which are composed by less calcite demanding phases, such as ye'elimite ($C_4A_3\bar{S}$) [2,3]. There are different ye'elimite-rich cements [4] such as Calcium SulphoAluminate (CSA) cements, which present more than 50 wt% of ye'elimite, and consequently release up to 37% less CO_2 than PC. However, they are expensive due to the need of high purity bauxite. In recent studies, dicalcium silicate-rich CSA cements, sometimes referred as Belite-Ye´elimite-Ferrite (BYF) cements, have been thought as the potential substitute of PC at large scales [5,6]. These BYF cements generally contain belite, C_2S (>50 wt%), as their main phase and ye'elimite (~30 wt%) as secondary phase. Some BYF cements (with the following composition: 33 wt% of β-C_2S and 19 wt% of orthorhombic-ye'elimite) develop low mechanical strengths [6] at intermediate ages, which is a technological disadvantage that has to be defeated.

The activation of BYF clinkers by stabilizing α'$_H$-polymorph of C_2S or getting modified β-C_2S, a distorted form due to the inclusion of foreign elements in the structure [7], may be the key to reach the objective of substituting PC [5,6,8,9]. In addition, cements with coexistence of alite, belite and ye'elimite (ABY) have also been examined to improve the final performances of BYF meanwhile CO_2 emissions are lower than PC [10–13]. Nevertheless, there are some problems concerning the clinkering of ABY binders since the optimum temperatures for the synthesis of alite and ye'elimite

are quite different. Alite formation is promoted by the appearance of melting phases, such as iron, silicates, and alkali sulfates [14], and requires at least 1350ºC, while ye'elimite starts its decomposition at 1300-1350ºC [15]. This can be addressed by using small amounts of fluorite (CaF_2) [16,17] in the raw mixture, which will act as flux and mineralizer, permitting the coexistence of both phases at temperatures ranging between 1250-1300ºC [14,15]. Moreover, the influence of zinc oxide on clinkering is described in the literature for PC and ABY [17–21]. The addition of ZnO promotes the formation of higher amounts of alite, which contains this element in its structure; in addition, it also stimulates physical changes in alite crystals: big and hexagonal alite crystals are transformed into smaller and elongated particles [21]. The addition of other mineralizers, such as MnO_2 [22] or P_2O_5 [23] on the phase composition during clinkering is also described in the literature.

In this work, the addition of different mineralizers and activators was studied to synthesize 5 g of standard clinker (alite-β-C_2S-ye'elimite). After that, the effect of borax on the phase assemblage of the clinker, named as αABY, (alite-(β and α'$_H$)-C_2S-ye'elimite) was studied (5 g). The raw material mixtures were reformulated to prepare, firstly 90 g, and finally, 2 kg of both clinkers. Both standard and αABY 2 Kg clinkers were characterized through laboratory X-ray powder diffraction (LXRPD) in combination with the Rietveld methodology, and field emission gun scanning electron microscopy (FEG-SEM) combined with energy dispersive X-ray spectrometry (EDS). The corresponding pastes and mortars, prepared with both 2 kg-clinkers were characterized. The hydration of the pastes was studied through LXRPD and thermal analyses, and the compressive strength of the corresponding mortars was measured and discussed.

2. Materials and Methods.

2.1 Clinker preparation.

Natural limestone and natural gypsum (both from Financiera y Minera cement factory, Spain), Kaolin (ref. NC-35 from Caolines Vimianzo, Spain), natural sand and iron ore (byproduct of the sulfuric acid industry) were used as raw materials. The addition of CaF_2 (99.0-102.0% pure, Sig*la*-Aldrich), $ZnSO_4 \cdot H_2O$ (≥99% pure, Sigma-Aldrich), $Na_2B_4O_7 \cdot 10H_2O$ (VWR, Prolabo), K_2CO_3 (99%, A.C.S) and Na_2CO_3 (99.999%, metal basis, Aldrich) was studied as mineralizers/activators. αABY clinkers contain both B_2O_3 and Na_2O, added as borax ($Na_2B_4O_7 \cdot 10H_2O$). Hereafter F, B, N and K stand for the amounts in weight percent of CaF_2, B_2O_3, Na_2O and K_2O added, respectively. Since all the studied mixtures contain 1.0 wt% of ZnO, that amount is not shown in the name of the clinkers. For instance, αABY_2F1B0.5N corresponds to a boron-bearing composition which contains 1.0 wt% of ZnO, 2.0 wt% of CaF_2, 1.0 wt% of B_2O_3 and 0.5wt% of Na_2O.

A first test to prepare the clinkers was performed by mixing the raw materials to obtain very small batches of approximately 5 grams. These resulting clinkers are named with the prefix ***sa-*** (small amount). For doing this, the raw materials were mixed by hand in an agate mortar for 30 min. After homogenization, raw materials were dye-pressed and molded into pellets of ~3 g of 20 mm diameter. Three of these pellets were placed in a Pt/Rh crucible and heated at 5°C/min up to 900°C and held at that temperature for 30 min. Then, the temperature was raised at the same rate up to 1300°C and held for 15 min. Finally, the clinkers were quenched using forced air convection. The resulting clinkers were ground and sieved until all the material goes through < 75 μm. For the preparation of higher amounts of clinker, the raw mixtures (~3 kg to obtain both standard and

αABY) were pre-homogenized for 90 min in a micro-Deval machine (A0655, Proeti S.A., Spain) at 100 rpm with steel balls (9 balls of 30 mm, 10 balls of 18 mm and 20 of balls of 10 mm). The procedure was performed in two steps. Firstly, the raw mixture was dye-pressed into pellets of 35 g and 55 mm of diameter and three of them were placed into a large Pt/Rh crucible. These pellets were also heated at 900°C and held for 30 min (heating rate of 5 °C/min). Then, they were further heated at 1300°C (at same heating rate) and held for 15 min. Finally, the samples were quenched using forced air convection. These resulting clinkers are named with the prefix ***ma-*** (medium amount) producing approximately 90 g. Finally, the second step consisted on the repetition of this procedure in several batches of six pellets, instead of three, to obtain ~2 kg of both standard and αABY. The resulting clinkers will be named with the prefix ***la-*** (large amount) to highlight the procedure to prepare 2 kg.

Standard and αABY *la*-clinkers were ground using a vibration disc mill to achieve similar particle/agglomerate size distribution (PSD). PSD measurements were carried out in a laser diffraction analyzer (MastersizerS, Malvern) provided with a dry sample cell.

2.2 Cement paste preparation.

Cements were prepared by mixing 14 wt% of anhydrite to both *la*-clinkers (standard and αABY) in a micro-Deval machine at 100 rpm, without any balls. Anhydrite was prepared by heating (700°C for 60 min) commercial autoclaved alpha bassanite from BELITH S.P.R.L. (Belgium).

Cement pastes were prepared with deionized water using a water-to-cement (w/c) mass ratio of 0.4 following UNE-EN 196-3 standard. To improve the workability, 0.4 wt% of the active matter

of a superplasticizer, SP, (polycarboxylate-based, Floadis 1623, with 25 wt% of active matter, Adex Polymer S.L., Madrid, Spain) was added to the pastes (referred to the cement content). That amount of SP provides the lowest viscosity values to the pastes. Both pastes were poured into hermetically closed cylinders of polytetrafluoroethylene (PTFE), and were rotated during the first 24 h (16 rpm) at 20±1ºC. After that, both samples were kept in water at 20 ± 1ºC for 1 and 28 days. Prior to laboratory X-Ray powder diffraction (LXRPD) characterization, the hydration of the cement pastes was stopped; for that, samples were firstly manually grinded, and after that, the powder was washed twice with isopropanol, and once with diethyl ether.

2.3 Mortar preparation.

Mortars were prepared according to UNE-EN196-1 at cement/sand and w/c ratios of 1/3 and 0.5, respectively, adding the same amount of superplasticizer (0.4 wt% referred to cement) selected for pastes. CEN EN196-1 standard sand was used. Mortar cubes ($3 \times 3 \times 3$ cm^3) were cast and cured at 20 ± 1°C and 99% relative humidity (RH) for 24 h. The cubes were demolded and kept in a water bath (20 ± 1°C) for 1 and 28 curing days until mechanical strength characterization (compression) was performed.

2.4 Laboratory X-Ray Powder Diffraction (LXRPD) data collection.

Patterns of all clinkers and pastes described above (after stopping hydration) were recorded on a PANalytical diffractometer, X'Pert MPD PRO model, located at Servicios Centrales de Apoyo a la Investigación (SCAI) at University of Malaga (Spain). It contains a Ge (111) primary Johansson

monochromator that provides strictly monochromatic CuKα_1 radiation (λ=1.54059Å) and a X'Celerator RTMS (Real Time Multiple Strip) detector, working in scanning mode with maximum active length. The X-ray tube worked at 45 kV and 40 mA. Patterns were collected from 5º to 70° (2θ) during ~2 hours using a spinning sample-holder (16 rpm) in order to enhance particle statistics.

A D8 ADVANCE DaVinci (Bruker AXS, Germany) diffractometer with a Molybdenum X-ray tube and a Johansson Ge(111) primary monochromator for monochromatic MoKα_1 radiation, λ=0.7093 Å was also used to collect the patterns of clinkers mixed with quartz as internal standard. The X-ray tube worked at 50 kV and 50 mA. The energy-dispersive linear detector LYNXEYE XE 500 μm, optimized for high energy radiation, was used with the maximum opening angle. Using these conditions, the samples were measured between 3-35º (2θ) with a step size of 0.020º and with a total measurement time of 4 hours by spinning the sample at 10 rpm.

2.5. LXRPD data analysis

The patterns were analyzed by Rietveld method using GSAS [24] software package, by using a pseudo-Voigt peak shape function with the asymmetry correction included [25,26], to obtain Rietveld Quantitative Phase Analysis (RQPA). The refined overall parameters were: background coefficients, phase scale factors, unit cell parameters, zero-shift error, peak shape parameters and preferred orientation coefficient if needed. The crystal structure descriptions used for all phases are given in Table 1 [27–38]. An internal standard approach was used to quantify the amorphous and crystalline non-quantified (ACn) content in the clinkers [39]. Quartz (99.56%, ABCR GmbH & Co. KG) was added to the samples as internal standard to a total content of ~20 wt%, and this

mixture was homogenized for 10 min in McCrone micronizing mill with isopropanol. The powder patterns of the clinkers mixed with quartz as internal standard were collected in the D8 ADVANCE diffractometer with Mo-radiation, as the microsabsorption phenomenon is minimized by high energy radiations [40]. On the other hand, the ACn content of the anhydrous cements and the pastes, at 1 and 28 days of hydration, was calculated using the external standard method (G-factor approach) [5] by using the X'Pert MPD PRO diffractometer.

2.6. Thermal analysis.

Differential thermal (DTA) and thermogravimetric (TGA) analyses were performed, for a ground fraction of every paste after stopping hydration, in a SDT-Q600 analyzer from TA instruments (New Castle, DE). The temperature increased from room temperature (RT) to 1000°C at a heating rate of 10°C/min. Measurements were performed in open platinum crucibles under air flow. The weighed loss from RT to 600°C was assumed to be water [41] (free and chemically bounded water) and that from 600 to 1000°C was considered as CO_2.

2.7. Field Emission Gun-Scanning Electron Microscopy (FEG-SEM)

The external surface and fracture cross-section of both *la*-clinker pellets were observed using a Jeol JSM-840 (Japan) scanning electron microscope (SEM). Prior to SEM observation, all the samples were gold sputtered.

In addition, *la*-clinker pellets were embedded in epoxy resin, and polished with diamond down to 3 μm. The elemental compositions were quantified by Field Emission Gun Scanning Electron

Microscopy (FEG-SEM) (FEI, Helios Nanolab 650). Backscattered Electron (BSE) images were taken at 15 kV with a retractable concentric backscatter (CBS) detector (annular solid-state device). EDS analysis was carried out with a X-Max 50 mm^2 detector (Oxford Instruments) with AZtec software (v.1.0). These samples were iridium sputtered. About 260 points were analyzed in every clinker.

2.8. Elemental analysis.

The elemental composition of raw materials and final clinkers was measured through X-ray fluorescence (XRF) using an ARL ADVANT'XP+ (Thermo Fisher) equipment. Boron and sodium contents in final clinkers were determined by inductively coupled plasma optical emission spectrometry (ICP-OES), using a 7300DV (Perkin Elmer) equipment. The elemental composition of each raw material is given in Table S1, as supplementary information. Table 2 gives the nominal elemental composition of the raw materials mixtures to produce *la*-standard (ABY) and also *sa*-, *ma*- and *la*- αABY alite-belite-ye'elimite clinkers (αABY).

2.9. Compressive strengths

The compressive strength of the cubic mortars (3 × 3 × 3 cm^3) was measured in a Model Autotest 200/10 W (Ibertest, Spain) press. Three cubic mortars were tested, at both studied hydration ages, to obtain the standard deviation values according to UNE-EN196-1. A corrector factor was applied to the measured values to properly compare with standard prisms (4 x 4 x 16 cm^3).

3. Results and discussion.

3.1. Clinkering.

The synthesis of *sa*-standard ABY clinker (5 g) with the addition of ZnO and CaF_2 was previously optimized [21], and following the same methodology, higher amounts of clinkers were prepared. In that work, it was demonstrated that the addition of CaF_2 resulted essential to obtain clinkers containing both alite and ye'elimite, and ZnO helped in the formation of higher amounts of alite. Because of that, both components are part of every raw mixture prepared in this work. Table 3 gives the mineralogical composition determined by Rietveld method of *sa*-, *ma*- and *la*- ABY clinkers (detailed in the experimental section) prepared according to [21], and the targeted composition is also included. The experimental mineralogical composition is close to the targeted one in all cases. As an example, Figure 1 gives the Rietveld plot for *la*-ABY_1F clinker, where the main peaks are labeled.

A step forward of the previous work [21] is to stabilize the α'-polymorph of C_2S. The main objective of this work consists on the determination of the type and amount of dopants to obtain a clinker with α'_H-polymorphs of C_2S. Table 4 shows the mineralogical composition of *sa*-αABY clinkers prepared following different attempts. It has been previously reported [7] that alkaline oxides stabilize alpha polymorphs (α-C_2S and α'_H-C_2S) in belite-rich Portland clinkers. However, the addition of 1.0 wt% of Na_2O (αABY_1F1N) or 2.0 wt% of K_2O (αABY_1F2K) did not yield

to the stabilization of any of the high temperature polymorphs of C_2S (as expected by [7]), see Table 4 and Figure S1, deposited as supplementary information. Consequently, this activation strategy was ruled out.

The role of borax as activator on belite sulfoaluminate clinkers has also been reported [5,42–44], therefore borax was added to the raw materials. According to previous studies [43,44], the addition of 2.0 wt% of B_2O_3 as borax was enough to stabilize all dicalcium silicate as α'_H-C_2S, in a clinker with more than 50 wt% of this phase. Consequently, αABY_1F2B0.9N clinker was prepared (containing 2.0 wt% of B_2O_3 and 1.0 wt% of Na_2O, Table 2). This clinker had the dicalcium silicate fully stabilized as α'_H-C_2S but the formation of alite was hindered, as expected [45], see Table 4. Therefore, the amount of borax was reduced to half, obtaining a clinker, αABY_1F1B0.5N, with a mixture of both polymorphs, α'_H-C_2S and β-C_2S, increasing the ratio β/α'_H from 0.0 to 0.14, but alite was still not formed. It is well known that CaF_2 increases the primary crystallization volume of C_3S, acting as a mineralizer [46]. Consequently, more fluorite (1.5 and 2.0 wt%) was added to the raw mixture to promote the formation of alite maintaining the stabilizing effect of boron on α'_H-polymorphs of C_2S. Mineralogical compositions of these two resulting clinkers, αABY_1.5F1B0.5N and αABY_2F1B0.5N, are given in Table 5. However, this synthetic strategy was only partly successful as just 4.8(2) wt% of alite was formed in the clinker with 2.0 wt% of fluorite, Table 5. Consequently, boron oxide was decreased down to 0.5 wt% and 0.3 wt% of B_2O_3, maintaining 1.0 wt% of CaF_2, to assure the burnability of the raw mixtures [21]. The ratio β/α'_H ratio increased as the percentage of B_2O_3 decreased, Table 4. The addition of 0.3 wt% of B_2O_3 was not desirable as that obtained ratio was ~13, Table 4. Finally, the raw mixture that contained 0.5 wt% of B_2O_3 allowed the preparation of a clinker containing the three targeted phases, i.e. with 15.3 wt% of α'_H-C_2S (β/α'_H=3.2), 9.7 wt% of alite and 13.4 wt% of ye'elimite, Table 4. The C_2S

contents of αABY clinkers are always higher than the alite amounts; however, the same nomenclature used for the standard clinkers, ABY, has been used here, αABY (instead of αBAY). Figure 2 shows the evolution of alite, C_2S (β and α'_H) and ye'elimite in *sa*-αABY clinker batches by adding different amounts of B_2O_3 as borax and CaF_2. By increasing the B_2O_3 content, from 0.2 to 2.0 wt% (when 1.0 wt% of CaF_2 was added), the amounts of alite and β-C_2S decrease, the α'_H-C_2S content increases considerably, and the ye'elimite amount is kept almost constant, Figure 2a. However, when the B_2O_3 content is kept constant (1.0 wt%) but the CaF_2 amount increases (from 1.0 to 2.0 wt%), alite and β-C_2S contents slightly increase, but α'_H-C_2S and ye'elimite amounts decrease, Figure 2b.

From the study reported above, αABY_1F0.5B0.3N composition was chosen to prepare medium amounts (90 g), by mixing appropriated amounts of raw materials with borax. The preparation of this clinker was carried out as previously detailed. Table 6 gives the mineralogical composition obtained for the intermediate step, i.e. *ma*-αABY_1F0.5B0.3N (3 pellets of 35 g each). Unfortunately, the amount of α'_H-C_2S was reduced by half when compared to the previous *sa*-clinkers (batches of 5 g), see Tables 4 and 6. Consequently, the amount of B_2O_3 (added as borax) was again updated under these experimental conditions. The increase of boron oxide from 0.5 wt% to 0.7 wt% yielded to a β/α'_H=0.8 but the amount of ye'elimite decreased, see Table 6, Figure 2 and Figure S2.

Finally, the amount of 0.6 wt% of B_2O_3 was chosen for the preparation of large amounts, 2 Kg, (6 pellets of 35 g each, and repeating the process several times), see Table 6 and Figure 3. Once 2 Kg of both clinkers were prepared, they were milled up to similar median particle size for a volume distribution ($D_{v,50}$ values of 7.9 and 8.9 μm for *la*-ABY_1F and *la*-αABY_1F0.6B0.3N, respectively). Figure S3, provided as Supplementary Information, shows the particle size

distribution (and cumulative curves) of both *la*-clinkers after milling. Both of them are polydisperse, where the *la*-ABY_1F powder shows a trimodal behavior (peaks centered at ~0.7, ~9 and ~60 μm), and the *la*-αABY_1F0.6B0.3N sample has a bimodal behavior (peaks centered at ~0.7 and ~10 μm). The values of D_{v10}, D_{v50} and D_{v90} of both powders are shown as an inset in Figure S3.

3.2. Microstructural analysis of *la*-clinkers.

Firstly, non-polished pellets of the *la*-clinkers were analyzed by SEM. Figures 4a and 4c show the micrographs of the external and the fracture surfaces, respectively, of *la*-ABY_1F clinker. Figures 4b and 4d show the corresponding micrographs for *la*-αABY_1F0.6B0.3N. Some conclusions can be drawn from this preliminary study: i) *la*-ABY_1F clinker is more porous than *la*-αABY_1F0.6B0.3N, Figures 4a and 4b, mainly due to the addition of borax in the latter which decreased the liquid phase appearance temperature [45] and favors the growth of the primary particle size; and ii) C_2S, which is present as rounded particles, is detected in both clinkers, with particle sizes lower than 5 μm in *la*-ABY_1F and about 10 μm in *la*-αABY_1F0.6B0.3N, Figures 4c and 4d, respectively, as previously observed [47,48]. Moreover, alite was primarily present as irregular angular crystals of ~30 μm in both clinkers (Figures 4b and 4c). The elongated shape of alite observed in LA-ABY_1Fwas also detected in a previous work [21], and was attributed to the presence of ZnO (Figures 4a and 4c). However, the addition of B_2O_3 seems to have hampered the development of this elongated shaped alite, favoring slightly larger angular particles of C_3S. For a deeper study, *la*-ABY_1F and *la*-αABY_1F0.6B0.3N clinkers were embedded in epoxi resin and

polished as detailed in the experimental section to be analyzed by EDS in the FEG-SEM microscope. Since the interaction volume is 1-2 μm^3, data have to be taken with caution and have to be considered as semiquantitative. Consequently, the discussion given below has to be considered as relative and not as absolute values. Figure 5 gives a triangle plot representing Al+Fe, Ca+Mg and Si+S atomic percentages for every measurement in each clinker. The theoretical values of these parameters for stoichiometric phases are also represented as solid blue symbols. The EDS measurements were clustered relatively close to the stoichiometric values; different symbols have been assigned: squares for C_3S, circles for C_2S, up-triangle for ye'elimite, rhombus for C_4AF, and down-triangle for CaF_2-$C_9S_3\overline{S}_3$. The micrographs displayed in Figure 6 were chosen to be representative of size and form of alite, C_2S (α'_H and β polymorphs), ferrite and ye'elimite crystals. A previous study [21] revealed that the addition of ZnO promoted the alite stabilization. Figure 7a shows the iron vs. sulfur content (atomic percentage), and Figure 7b shows the zinc atomic percentage vs. fluorine atomic percentages, of the EDS data obtained from both *la*-clinkers. Here, the same symbol labeling, as in Figure 5 has been followed. The theoretical values have also been included for the sake of comparison. This representation reveals that Fluorellestadite contains the higher amounts of fluorine, as expected. Moreover, it can be observed that Zn and remaining F are mainly incorporated into ferrite, where both clinkers show the same tendency. Alite contains more zinc than C_2S (α'_H and β polymorphs) as expected [21]. Furthermore, sulfur is mostly incorporated into Fluor-ellestadite, ye'elimite and, in lower percentages, in C_2S (both α'_H and β polymorphs and ferrite [49].

From the EDS study, experimental formulations for alite and belite were determined. To calculate the chemical composition of alite, it was assumed that Mg^{2+} substitutes Ca and that Al^{3+} was placed in both the Ca and Si sites [50] giving $Ca_{2.64}Mg_{0.06}Al_{0.05}(Si_{0.95}Al_{0.05})O_{4.75}$ formula. On the other

hand, belite chemistry composition was determined by assuming that both Al^{3+} and sulfur substituted Si [51] giving $Ca_{1.79}(Si_{0.85}Al_{0.08}S_{0.07})O_{3.81}$ chemical formula. Unfortunately, in the EDS analysis of *la*-αABY_1F0.6B0.3N it was not possible to distinguish between β and α'_H C_2S.

3.3. Elemental analysis of final clinkers.

Table 7 shows the mineralogical composition (in weight percentage) determined by RQPA, including the ACn content, of the *la*-ABY_1F and *la*-αABY_1F0.6B0.3N clinkers, after preparing 2 kg of each clinker. The final composition of these *la*-clinkers is quite similar to that found for the corresponding *ma*-clinkers (Tables 3 and 6), taking into account that the former data include ACn content, confirming the reproducibility of the method.

A deeper study on the composition of the *la*-clinkers was performed. Table 8 gives the elemental composition, expressed in weight percentage of oxides, of the final clinkers obtained by XRF and ICP techniques. When these data (XRF+ICP column) are compared with the nominal elemental composition of the raw mixtures (also included in Table 8), it can be deduced that part of the sulfur was lost during the clinkering of both materials. Consequently, as all the elemental compositions as normalized to 100%, the remaining element contents seems to be partially overestimated when compared to the nominal composition.

We have also included in Table 8 the derived elemental composition calculated from RQPA reported in Table 7. The calculated chemical formulas for alite and belite from EDS study were used for this calculation. The elemental composition of the ACn can be estimated by the difference

between the elemental composition obtained from XRF & ICP and the derived elemental composition from RQPA, Table 8. The negative value of the percentage of SiO_2 of ACn in *la*-αABY_1F0.6B0.3N may be related to semiquantitative EDS analyses performed, that gave approximate stoichiometries for alite and dicalcium silicate phases. In order to properly compare the chemical nature of both ACn contents, data from Table 8 have been renormalized to 100 wt% of oxides, not taking into account the negative values, and are shown in Table 9. These values indicate that ACn elemental composition is close to amorphous calcium aluminates in both clinkers. However, *la*-αABY_1F0.6B0.3N amorphous phase contains slightly more amount of minor elements different from Ca and Al. Moreover, the amount of ACn in both clinkers is also very similar and low, taking into consideration that the quantification of amorphous contents below 10 wt% are subjected of higher errors [52].

3.4. Hydration of *la*-ABY_1F and *la*-αABY_1F0.6B0.3N cements

It has been proved that the addition of boron and sodium yield to the stabilization of α'_H C_2S. Moreover, this addition has promoted the disappearance of the elongated particles (a change in the morphology) and bigger rounded ones (a change in size), as shown in Figures 6c and 6d. To determine the effect of these facts on the hydration of both cements, pastes and mortars were prepared. Table 10 shows the phase assemblage of both cement pastes at 0, 1 and 28 days of hydration, including ACn and free water (FW) contents. ACn was determined by the external standard methodology as detail in the experimental section. FW was calculated by analyzing DTA-TGA curves of stopped pastes by using this equation:

$$FW = W_T - \frac{BW_{ATD} x CM}{100 - BW_{ATD}},$$

where BW_{ATD} is the loss up to 600ºC from DTA-TGA curves (given in Table S2 as supplementary information), W_T is the total amount of initially added water (33.33 wt%) and CM is the weight percentage of cement used (66.67 wt%).

As explained before, the addition of borax to the raw materials not only helps the formation of α'_H-C_2S, but also modifies the phase assemblage (by decreasing the amount of alite and ye'elimite) and the size (by increasing the rounded particles) of the phases. Consequently, these effects may cause different hydration behaviors. The amount of ACn content of the cements at 0 days, Table 10, are higher than those obtained for the clinkers mainly due to the addition of anhydrite and the milling process.

During hydration, the content of anhydrous phases is diminishing with time, in both cements, and the content of hydration phases is increasing. On the one hand, α'_H-C_2S reacts at a higher pace at 1d of hydration than β-C_2S in the *la*-αABY_1F0.6B0.3N paste, as expected, where the degree of reaction of α'_H-C_2S is ~11 while β-C_2S has not reacted at 1d. Moreover, the degree of reaction of β-C_2S is also different in both cements. While this polymorph in *la*-ABY_1F clinker achieves ~34% of degree of reaction after 28 days; in *la*-αABY_1F0.6B0.3N the value is close to 74%, confirming that the different hydration environment also has enhanced the hydraulic behavior of C_2S. On the other hand, initially, the *la*-ABY_1F paste contains higher amounts of alite and ye'elimite. The reaction degrees of alite and ye'elimite after 1 day of hydration, ~50% and ~78%, respectively, are higher in the *la*-ABY_1F paste than in the *la*-αABY_1F0.6B0.3N paste, ~26% and ~26%, respectively. At 1 day of hydration, the AFt content quantified in the *la*-ABY_1F paste is higher than that found in the *la*-αABY_1F0.6B0.3N paste. In addition, the former shows a lower amount of free water, Table 10, which is also related with the higher degree of reactivity of ABY; this is in agreement with the lower primary particle size of the phases. Table 10 includes the

expected mineralogical composition (including FW and ACn). These values have been calculated by taking into account the actual degree of reaction of C_3S and C_2S polymorphs by using the following reactions [53]:

$C_3S + 5.2\ H \rightarrow C_{1.8}SH_4 + 1.2\ CH$

$C_2S + 4.2\ H \rightarrow C_{1.8}SH_4 + 0.2\ CH$

Moreover, it is well known that in the presence of silicate the hydration of ye'elimite phase can take two alternatives [54]:

$C_4A_3\overline{S} + 8\ C\overline{S} + 6\ CH + 90\ H \rightarrow 3\ C_6A\overline{S}_3H_{32}$

$C_4A_3\overline{S} + 2\ C\overline{S} + 38\ CH + 90\ H \rightarrow C_6A\overline{S}_3H_{32} + 4\ AH_3$

It has been assumed that ye'elimite reacts at 50% by the first equilibrium and 50% in the second one, in both cements.

The reactivity of mayenite in *la*-αABY_1F0.6B0.3N paste follows [55]:

$C_{12}A_7 + 12\ C\overline{S}H_2 + 113\ H \rightarrow 4\ C_6A\overline{S}_3H_{32} + 3\ AH_3$

For the sake of simplicity, we have considered that C_4AF is not reacting. It has to be taken into account that all $C_{1.8}SH_4$ and AH_3 has been included as ACn in table 10. The expected composition match very well the experimentally obtained values in both cement pastes. The higher amount of expected ettringite may be due to its decomposition (experimentally observed) which will increase the amount of amorphous and AFm. The expected amount of free water is slightly higher than the experimentally measured because in the calculations C_4AF has not been taken into account.

The difference in degree of reactions between both cement pastes justify the higher mechanical strengths (compression) measured for the *la*-ABY_1F mortars at 1 day of hydration, Figure 8 (and table as an inset). However, at 28 days of hydration, the compressive strength of *la*-αABY_1F0.6B0.3N mortars is much higher, Figure 8. This is related to the higher β-C_2S contents,

which reacts at higher ages, and also the presence of the more reactive phase of α'_{H}-C_2S. This is in agreement with lower free water content quantified at this age, Table 10. It is worth to highlight the high values of compressive strengths achieved by the *la*-αABY_1F0.6B0.3N mortar at 28 days (75 ± 2 MPa).

4. Conclusions

In this study, 2 kg of standard ABY clinker, with coexistence of C_3S and $C_4A_3\overline{S}$, were prepared by adding 1 wt% of CaF_2 and 1 wt% of ZnO and heated up in a two steps procedure (900ºC/30 min and 1300ºC/15min) followed by a quenching in batches of 90 grams.

Furthermore, the stabilization of α-forms of belite by adding dopants to the standard raw mixture has been obtained by adding 0.6 wt% of B_2O_3 and 0.3 wt% of Na_2O, as borax, to the raw mixture, which also contained 1 wt% of CaF_2 and 1 wt% of ZnO. The addition of other elements such as Na_2O or K_2O, or higher amounts of borax was ruled out as no stabilization was achieved.

The EDS study revealed that, in both clinkers, Zn and F are mainly incorporated into ferrite and alite, and sulfur is preferably incorporated into Fluor-ellestadite, ye'elimite and, in lower concentrations, in belite and ferrite. The elemental composition of the amorphous fraction of the clinkers has been determined by a joint study of XRF data and EDS-semiquantitative results. ACn elemental composition is close to amorphous calcium aluminates in both clinkers; while *la*-αABY_1F0.6B0.3N amorphous phase contains slightly more amount of minor elements different from Ca and Al.

Finally, mortars prepared using the standard clinker show higher compressive strengths than the boron-bearing one at 1 day of hydration, due to the higher ye'elimite and alite contents, jointly

with the lower particle size of the phases. However, at 28 hydration days, mortars prepared with the boron-bearing clinker show very high compressive strength values, much higher than those for the standard mortars, which is related to the presence of α'_H belite.

5. Acknowledgements

This work is part of the PhD of Mr. Jesus D. Zea-Garcia. This work was supported by Spanish MINECO and FEDER [BIA2017-82391-R research project and I3 [IEDI-2016-0079] program].

Appendix A. Supplementary data

Supplementary data associated with this article can be found, in the online version, at *(in the submission stage the supplementary material is submitted as e-component as a doc file).*

Raw XRPD patterns analyzed in this article can be found online on Zenodo at https://doi.org/10.5281/zenodo.1304464 and used under the Creative Commons Attribution license.

Figure captions

Figure 1. LXRPD Rietveld plot for *la*-ABY_1F clinker, with main peaks labelled.

Figure 2. Evolution of alite, belite (β and α'_H) and ye'elimite (wt%) in the *sa*-αABY clinker batches (5 g) by adding different amounts of (a) B_2O_3 and (b) CaF_2.

Figure 3. LXRPD Rietveld plot for *la*-αABY_1F0.6B0.3N clinker, with main peaks labelled.

Figure 4. SEM micrographs for (a) and (c) *la*-ABY_1F and (b) and (d) *la*-αABY_1F0.6B0.3N at different magnifications, being (a) and (b) the external surface and (c) and (d) the fracture surface.

Figure 5. Triangle plot of EDS measurements of *la*-ABY_1F (black empty symbols) and *la*-αABY_1F0.6B0.3N (red empty symbols) where Al+Fe, Si+S and Ca+Mg atomic percentages are represented. Blue solid symbols stand for the theoretical values for stoichiometric phases. Square: alite; circle: belite; up-triangle: ye'elimite; rhombus: ferrite; down-triangle: fluor ellestadite.

Figure 6. Polished cross-section SEM micrographs of (a) *la*-ABY_1F and (b) *la*-αABY_1F0.6B0.3N. Symbols as in Figure 5.

Figure 7. EDS measurements: (a) Zn vs. F atomic percentages and (b) Fe vs. S atomic percentages of *la*-ABY_1F and *la*-αABY_1F0.6B0.3N. Symbols as in Figure 5.

Figure 8. Compressive strengths values of mortars prepared with standard-*la*-ABY_1F and *la*-αABY_1F0.6B0.3N clinkers at 1 and 28 hydration days.

Table 1. Bibliographic information and ICSD collection codes for all phases used for Rietveld refinements.

Name	Polymorph/Phase	ICSD Codes	Biblio. Ref.
Alite	M_3-C_3S	94742	[27]
Belite	α'_H-C_2S	431571	[28]
	β-C_2S	81096	[31]
Ye'elimite	*o*-$C_4A_3\overline{S}$	237892	[32]
	c-$C_4A_3\overline{S}$	194482	[33]
Brownmillerite (Ferrite)	C_4AF	9197	[34]
Tricalcium aluminate	*c*-C_3A	1841	[35]
Mayenite	*c*-$C_{12}A_7$	241243	[36]
Fluor-ellestadite	CaF_2-$C_9S_3\overline{S}_3$	97203	[37]
Calciolangbeinite	$C_2K\overline{S}_3$	40989	[38]
Lime (CaO)	C	52783	[29]
Periclase (MgO)	M	9863	[30]

Table 2. Nominal elemental compositions, expressed in weigh percentage of oxides excluding water and CO_2, of all **raw mixtures** used to prepare ABY and αABY clinkers. Prefix ***sa-*** means "small amount" (3 pellets of 3 g each), ***ma-*** means "medium amount" (3 pellets of 35 g each), ***la-*** means "large amount" (6 pellets of 35 g each).

Clinker	CaO	SiO_2	Al_2O_3	SO_3	Fe_2O_3	MgO	K_2O	Na_2O	ZnO	CaF_2	B_2O_3
***la*-ABY_1F**	58.9	19.8	10.7	5.4	1.6	0.8	0.8	--	1.0	1.0	--
***sa*-αABY_1F1N**	58.3	19.6	10.6	5.3	1.6	0.8	0.8	**1.0**	1.0	1.0	--
***sa*-αABY_1F2K**	58.2	19.6	10.5	5.3	1.6	0.8	**2.0**	--	1.0	1.0	--
***sa*-αABY_1F2B0.9N**	57.2	19.2	10.4	5.2	1.5	0.8	0.8	**0.9**	1.0	1.0	**2.0**
***sa*-αABY_1F1B0.5N**	58.0	19.5	10.5	5.3	1.6	0.8	0.8	**0.5**	1.0	1.0	**1.0**
***sa*-αABY_1.5F1B0.5N**	57.7	19.4	10.5	5.3	1.6	0.8	0.8	**0.5**	1.0	1.5	**1.0**
***sa*-αABY_2F1B0.5N**	57.4	19.3	10.4	5.2	1.5	0.8	0.8	**0.5**	1.0	2.0	**1.0**
***sa*-αABY_1F0.5B0.3N**	58.5	19.7	10.6	5.3	1.6	0.8	0.8	**0.3**	1.0	1.0	**0.5**
***sa*-αABY_1F0.3B0.1N**	58.7	19.7	10.6	5.3	1.6	0.8	0.8	**0.1**	1.0	1.0	**0.3**
***ma*-αABY_1F0.5B0.3N**	58.5	19.7	10.6	5.3	1.6	0.8	0.8	0.3	1.0	1.0	0.5
***ma*-αABY_1F0.7B0.4N**	58.2	19.6	10.5	5.3	1.6	0.8	0.8	**0.4**	1.0	1.0	**0.7**
***ma*-αABY_1F0.6B0.3N**	58.4	19.6	10.6	5.3	1.6	0.8	0.8	**0.3**	1.0	1.0	**0.6**
***la*-αABY_1F0.6B0.3N**	58.4	19.6	10.6	5.3	1.6	0.8	0.8	**0.3**	1.0	1.0	**0.6**

Table 3. Mineralogical composition of standard ABY clinkers obtained by RQPA. The targeted mineralogical composition is also included. Prefix ***sa-*** means "small amount" (3 pellets of 3 g each), ***ma-*** means "medium amount" (3 pellets of 35 g each), ***la-*** means "large amount" (6 pellets of 35 g each). Numbers between brackets are mathematical errors from Rietveld fits (not standard deviation).

phases	*Targeted*	*sa*-ABY_1F	*ma*-ABY_1F	*la*-ABY_1F
C_3S-M_3	*45.0*	29.5(1)	37.5(2)	**41.5(2)**
β-C_2S	*25.0*	44.3(2)	32.8(2)	**28.4(3)**
γ-C_2S	--	--	--	--
α'_H-C_2S	--	--	--	--
o-$C_4A_3\overline{S}$	*20.0*	10.5(3)	10.0(3)	**9.3(3)**
c-$C_4A_3\overline{S}$		7.3(3)	7.4(3)	**8.1(3)**
C_4AF	*5.0*	4.6(2)	4.1(1)	**3.8(1)**
$C\overline{S}$	*5.0*	--	0.5(1)	**0.4(1)**
C_3A	--	1.5(1)	0.4(1)	**0.3(1)**
$C_{12}A_7$	--	--	--	**0.6(1)**
CaF_2-$C_9S_3\overline{S}_3$	--	0.4(1)	4.2(2)	**4.3(2)**
CaO	--	--	1.2(1)	**1.9(1)**
MgO	--	--	1.0(1)	--
$C_2K\overline{S}_3$	--	1.8(1)	1.0(1)	**1.5(1)**

Table 4. Mineralogical composition (in weight percentage) determined by Rietveld method of *sa*-αABY clinkers, doped with alkaline oxides and borax. Batches of 5 g (3 pellets of 3 g each) were prepared. Numbers between brackets are mathematical errors from Rietveld fits (not standard deviation)

	αABY_1F1N	αABY_1F2K	αABY_1F2B0.9N	αABY_1F1B0.5N	**αABY_1F0.5B0.3N**	αABY_1F0.3B0.1N
C_3S-M_3	31.6(2)	30.5(2)	--	--	**9.6(1)**	18.1(2)
β-C_2S	44.9(2)	39.0(2)	--	9.0(3)	**49.4(2)**	52.1(2)
γ-C_2S	--	--	1.5(2)	0.5(1)	**--**	0.8(1)
α'$_H$-C_2S	--	--	73.2(1)	64.7(1)	**15.1(3)**	3.9(4)
o-$C_4A_3\overline{S}$	6.3(4)	5.2(3)	9.8(4)	6.4(4)	**7.4(2)**	8.8(3)
c-$C_4A_3\overline{S}$	4.3(4)	5.4(3)	3.2(4)	3.0(4)	**6.0(3)**	7.4(3)
C_4AF	2.8(2)	3.7(1)	5.3(2)	3.8(1)	**4.5(2)**	4.0(1)
$C\overline{S}$	--	--	--	--	**--**	--
C_3A	1.5(1)	1.3(1)	2.2(1)	6.2(1)	**4.3(1)**	1.8(1)
$C_{12}A_7$	7.3(2)	7.6(1)	2.6(1)	3.1(1)	**0.5(1)**	--
CaO	--	--	--	--	**--**	--
MgO	--	--	--	--	**--**	--
CaF_2-$C_9S_3\overline{S}_3$	--	--	1.4(2)	1.9(1)	**1.2(2)**	1.2(2)
$C_2K\overline{S}_3$	1.3(1)	6.8(2)	1.0(1)	1.3(2)	**2.1(1)**	2.0(1)

Table 5. Effect of calcium fluoride content (1.5 and 2.0 wt%) on the phases of *sa*-αABY clinker. Batches of 5 g (3 pellets of 3 g each) were prepared. Numbers between brackets are mathematical errors from Rietveld fits (not standard deviation)

	αABY_1.5F1B0.5N	**αABY_2F1B0.5N**
C_3S-M_3	0.8(1)	4.8(2)
β-C_2S	12.2(3)	14.7(3)
γ-C_2S	--	1.6(1)
α'$_H$-C_2S	58.9(2)	50.1(2)
o-$C_4A_3\overline{S}$	4.6(3)	2.5(2)
c-$C_4A_3\overline{S}$	3.3(3)	2.0(2)
C_4AF	4.5(2)	4.5(2)
$C\overline{S}$	1.0(1)	1.5(1)
C_3A	4.7(2)	2.1(2)
$C_{12}A_7$	6.3(1)	10.9(1)
CaO	--	--
MgO	--	--
CaF_2-$C_9S_3\overline{S}_3$	2.6(1)	4.1(1)
$C_2K\overline{S}_3$	1.0(1)	1.1(1)

Table 6. Mineralogical composition (in weight percentage) determined by RQPA of αABY clinkers doped with different amounts of borax. Prefix ***sa-*** means "small amount" (3 pellets of 3 g each), ***ma-*** means "medium amount" (3 pellets of 35 g each), ***la-*** means "large amount" (6 pellets of 35 g each to produce 2 kg). Numbers between brackets are mathematical errors from Rietveld fits (not standard deviation)

Phases	***ma-*** **αABY_1F0.5B0.3N**	***ma-*** **αABY_1F0.7B0.4N**	***ma-*** **αABY_1F0.6B0.3N**	***la-*** **αABY_1F0.6B0.3N**
C_3S-M_3	21.4(2)	9.1(2)	15.5(2)	**15.7(2)**
β-C_2S	44.7(2)	28.9(3)	36.6(2)	**41.8(2)**
γ-C_2S	--	--	--	**--**
α'$_H$-C_2S	8.2(3)	36.4(2)	22.6(3)	**18.0(3)**
o-$C_4A_3\overline{S}$	6.0(2)	3.4(2)	5.9(5)	**2.9(2)**
c-$C_4A_3\overline{S}$	5.0(2)	3.4(2)	3.2(5)	**4.8(2)**
C_4AF	3.8(1)	3.1(1)	3.3(1)	**3.2(1)**
$C\overline{S}$	--	--	--	**--**
C_3A	1.7(1)	3.4(2)	2.6(2)	**2.4(2)**
$C_{12}A_7$	5.5(1)	7.3(1)	4.7(1)	**6.6(1)**
CaO	--	--	1.0(1)	**1.0(1)**
MgO	--	--	--	**--**
CaF_2-$C_9S_3\overline{S}_3$	3.5(2)	4.2(2)	3.6(2)	**3.1(2)**
$C_2K\overline{S}_3$	1.2(1)	0.9(1)	0.8(1)	**0.6(1)**

Table 7. Mineralogical composition (in weight percentage) determined by RQPA of *la*-ABY_1F and *la*-αABY_1F0.6B0.3N clinkers, including the ACn. These are the clinkers prepared in large amount, i.e. 6 pellets of 35 g each to produce 2 kg. Numbers between brackets are mathematical errors from Rietveld fits (not standard deviation)

Phases	*la*-ABY_1F	*la*-αABY_1F0.6B0.3N
C_3S-M_3	32.6(3)	14.4(3)
β-C_2S	30.4(4)	37.1(4)
α'_H-C_2S	--	18.5(5)
o-$C_4A_3\overline{S}$	9.8(8)	2.8(7)
c-$C_4A_3\overline{S}$	5.8(8)	4.7(7)
C_4AF	4.3(2)	3.9(2)
$C\overline{S}$	--	--
C_3A	--	--
$C_{12}A_7$	1.2(1)	7.7(2)
CaO	--	--
MgO	--	--
CaF_2-$C_9S_3\overline{S}_3$	3.5(3)	4.2(4)
$C_2K\overline{S}_3$	--	--
ACn	12.6(2)	6.6(2)

Table 8. Nominal elemental composition (as in Table 2), direct (from XRF and ICP) and derived (from LXRPD) elemental analyses, expressed as oxide weight percentages, of *la*-ABY_1F and *la*-αABY_1F0.6B0.3N clinkers.

	***la*-ABY_1F**							
	Nominal Elemental composition	**XRF & ICP**	**Crystalline fraction from LXRPD#**	**Amorphous fraction from LXRPD***	**Nominal Elemental composition**	**XRF & ICP**	**Crystalline fraction from LXRPD#**	**Amorphous fraction from LXRPD***
	wt%	**wt%**	**wt%**	**wt% *la*-αABY_1F0.6B0.3N**	**wt%**	**wt%**	**wt%**	**wt%**
CaO	*58.9*	58.9	51.6	7.3	*58.4*	58.6	55.2	3.3
SiO_2	*19.8*	20.1	19.0	1.1	*19.6*	19.8	22.1	-2.3
Al_2O_3	*10.7*	12.3	10.9	1.4	*10.6*	12.2	9.9	2.3
SO_3	*5.4*	3.6	3.9	-0.3	*5.3*	3.4	3.2	0.2
Fe_2O_3	*1.6*	1.5	1.4	0.1	*1.6*	1.6	1.3	0.3
MgO	*0.8*	1.1	0.4	0.7	*0.8*	1.1	0.2	0.9
ZnO	*1*	1.0	--	1.0	*1*	1.0	--	1.0
K_2O	*0.8*	0.5	--	0.5	*0.8*	0.5	--	0.5
Na_2O	--	0.0	--	--	***0.3***	0.3	0.5	-0.2
CaF_2	*1*	1.0	0.3	0.7	*1*	1.0	0.3	0.7
B_2O_3	--	0.0	--	--	***0.6***	0.6	0.6	--
Total	*100*	100	87.4	12.6	*100*	100	93.4	6.6

*Elemental composition of ACn fraction = elemental composition from XRF&ICP – Elemental composition of the crystalline fraction
#Stoichiometric phases have been used for calculations, except: $Ca_{2.64}Mg_{0.06}Al_{0.05}(Si_{0.95}Al_{0.05})O_{4.75}$ for alite and $Ca_{1.79}(Si_{0.85}Al_{0.08}S_{0.07})O_{3.75}$ for β-belite, both obtained from the EDS-FEG-SEM study, and $Ca_{1.85}Na_{0.15}(SiO_4)_{0.85}(BO_3)_{0.15}$ for α'_H-belite from [28]

Table 9. Derived (from LXRPD) elemental analyses, expressed as oxide weight percentages, of the amorphous fraction of *la*-ABY_1F and *la*-αABY_1F0.6B0.3N clinkers, normalized to 100 wt%.

	***la*-ABY_1F**	***la*-αABY_1F0.6B0.3N**
	wt%	**wt%**
CaO	57	36
SiO_2	9	--
Al_2O_3	11	25
SO_3	--	2
Fe_2O_3	1	3
MgO	5	10
ZnO	8	11
K_2O	4	5
Na_2O	--	--
CaF_2	5	8
B_2O_3	--	--
total	*100*	*100*

Table 10. Rietveld quantitative phase analysis results in weight percentage (including ACn and FW) for *la*-ABY_1F and *la*-αABY_1F0.6B0.3N pastes, with w/c = 0.50 and 0.4 wt% SP, as a function of hydration. Numbers between brackets are mathematical errors from Rietveld fits (not standard deviation)

	***la*-ABY_1F**				***la*-αABY_1F0.6B0.3N**			
Phases	**0d**	**1d**	**28d**	***Calculated 28d***	**0d**	**1d**	**28d**	***Calculated 28d***
C_3S-M_3	17.4(3)	7.7(2)	1.1(3)	*1.1*	5.8(3)	4.3(2)	0.7(2)	*0.7*
β-C_2S	15.3(4)	15.1(3)	10.6(3)	*10.6*	17.9(3)	18.6(2)	4.7(4)	*4.7*
α'$_H$-C_2S	-	-	-		8.7(4)	5.4(3)	1.1(3)	*1.1*
o-$C_4A_3\overline{S}$	3.7(5)	0.9(3)	-	-	1.8(3)	2.6(1)	-	-
c-$C_4A_3\overline{S}$	4.4(5)	0.8(3)	-	-	2.6(4)	-	-	-
C_4AF	2.3(2)	1.8(1)	-	*2.3*	1.7(2)	1.6(2)	-	*1.7*
$C\overline{S}$	9.1(3)	-	-	*0.1*	9.1(3)		-	*0.5*
$C_{12}A_7$	-	-	-		3.1(2)	1.2(1)	-	-
MgO	0.5(1)	-	-	*0.5*	-	-	-	
CaF_2-$C_9S_3\overline{S}_3$	1.1(3)	1.0(3)	1.0(3)	*1.1*	1.0(4)	1.6(1)	0.6(3)	*1.0*
AFt	-	28.0(2)	25.2(2)	*33.3*	-	23.6(2)	27.2(2)	*29.2*
AFm	-	0.2(1)	2.7(7)	-	-	-	4.0(8)	-
CH	-	0.4(1)	2.0(1)	*3.8*	-	-	1.9(1)	*2.2*
Katoite	-	-	1.4(4)	-	-	-	0.8(2)	-
ACn	12.8	29.6	48.6	*12.8$^{\&}$+25.1**	15.0	22.0	54.3	*15$^{\&}$+34.8**
Free Water	33.3	14.5	7.3	*9.3*	33.3	19.0	4.7	*9.1*

$^{\&}$Initial ACn content of the clinker; *ACn from hydration, i.e. C-S-H gel and AH_3.

REFERENCES

[1] I. Amato, Green cement: Concrete solutions, Nature. 494 (2013) 300–301. doi:10.1038/494300a.

[2] E. Gartner, H. Hirao, A review of alternative approaches to the reduction of CO2 emissions associated with the manufacture of the binder in concrete., Cem. Concr. Res. 78 (2015) 126–142.

[3] G. Belz, J. Beretka, M. Marroccoli, L. Santoro, N. Sherman, G.L. Valenti, Use of Fly Ash, Blast Furnace Slag, and Chemical Gypsum for the Synthesis of Calcium Sulfoaluminate-Based Cements, Spec. Publ. 153 (1995) 513–530. doi:10.14359/1086.

[4] M.A.G. Aranda, A.G. De la Torre, Sulfoaluminate cement in Eco-efficient concrete; Pacheco-Torgal, F. Ed.; Jalali, S. Ed. Labrincha, J. Ed., Woodhead Publ. Cambridge. (2013) 488–522.

[5] G. Álvarez-Pinazo, A. Cuesta, M. García-Maté, I. Santacruz, E.R. Losilla, A.G. De La Torre, L. León-Reina, M.A.G. Aranda, Rietveld quantitative phase analysis of Yeelimite-containing cements, Cem. Concr. Res. 42 (2012) 960–971. doi:10.1016/j.cemconres.2012.03.018.

[6] V. Morin, P. Termkhajornkit, B. Huet, G. Pham, Impact of quantity of anhydrite, water to binder ratio, fineness on kinetics and phase assemblage of belite-ye'elimite-ferrite cement, Cem. Concr. Res. 99 (2017) 8–17. doi:10.1016/j.cemconres.2017.04.014.

[7] K. Morsli, Á.G. De La Torre, S. Stöber, A.J.M. Cuberos, M. Zahir, M.A.G. Aranda, Quantitative phase analysis of laboratory-active belite clinkers by synchrotron powder diffraction, J. Am. Ceram. Soc. 90 (2007) 3205–3212.

[8] I. Jelenić, A. Bezjak, M. Bujan, Hydration of B2O3-stabilized α′-and β-modifications of dicalcium silicate, Cem. Concr. Res. 8 (1978) 173–180. doi:10.1016/0008-8846(78)90006-6.

[9] W.-H. Chae, D.-C. Park, S.-H. Choi, The Korean journal of ceramics., Korean J. Ceram. 2 (1996) 147–151. http://www.ndsl.kr/ndsl/search/detail/article/articleSearchResultDetail.do?cn=NART56198483 (accessed June 29, 2018).

[10] N. Chitvoranund, B. Lothenbach, F. Winnefeld, C.W. Hargis, Synthesis and hydration of alite-calcium sulfoaluminate cement, Adv. Cem. Res. (2016).

[11] S. Ma, R. Snellings, X. Li, X. Shen, K.L. Scrivener, Alite-ye'elimite cement: Synthesis and mineralogical analysis, Cem. Concr. Res. 45 (2013) 15–20. doi:10.1016/j.cemconres.2012.10.020.

[12] R. Lili, L. Xiaocun, Q. Tao, L. Jian, Z. Deli, L. Yanjun, Influence of MnO2 on the Burnability and Mineral Formation of Alite-sulphoaluminate Cement Clinker, Silic. Ind. 74 (2009) 183–188.

[13] D. Londono-Zuluaga, J.I. Tobon, M.A.G. Aranda, I. Santacruz, A.G. De La Torre, Clinkering and hydration of Belite-Alite-Ye´elimite cement, Cem. Concr. Compos. 80 (2017) 333–341. doi:10.1016/j.cemconcomp.2017.04.002.

[14] M.A.G. Aranda, A.G. De La Torre, K. Morsli, M. Zahir, In-situ Clinkerization Study of Belite Portland Clinkers by Synchrotron X-ray Powder Diffraction, 12th Int. Congr. Chem. Cem. (2007).

[15] Á.G. De La Torre, A.J.M. Cuberos, G. Álvarez-Pinazo, A. Cuesta, M.A.G. Aranda, In situ powder diffraction study of belite sulfoaluminate clinkering, J. Synchrotron Radiat. 18 (2011) 506–514.
[16] I.A. Altun, Effect of CaF2 and MgO on sintering of cement clinker, Cem. Concr. Res. 29 (1999) 1847–1850. doi:10.1016/S0008-8846(99)00151-9.
[17] J.H. Li, H.W. Ma, H.W. Zhao, Preparation of Sulphoaluminate-Alite Composite Mineralogical Phase Cement Clinker from High Alumina Fly Ash, Key Eng. Mater. 334–335 (2007) 421–424. doi:10.4028/www.scientific.net/KEM.334-335.421.
[18] H.-M. Ludwig, W. Zhang, Research review of cement clinker chemistry, Cem. Concr. Res. 78 (2015) 24–37. doi:10.1016/j.cemconres.2015.05.018.
[19] X. Li, X. Shen, J. Xu, X. Li, S. Ma, Hydration properties of the alite – ye'elimite cement clinker synthesized by reformation, Constr. Build. Mater. 99 (2015) 254–259. doi:10.1016/j.conbuildmat.2015.09.040.
[20] H. Zhang, I. Odler, Investigations on high SO3 Portland clinkers and cements II. Properties of cements, Cem. Concr. Res. 26 (1996) 1315–1324. doi:10.1016/0008-8846(96)00129-9.
[21] R. Pérez-Bravo, G. Álvarez-Pinazo, J.M. Compana, I. Santacruz, E.R. Losilla, S. Bruque, Á.G. De la Torre, Alite sulfoaluminate clinker: Rietveld mineralogical and SEM-EDX analysis, Adv. Cem. Res. 26 (2014) 10–20. doi:10.1680/adcr.12.00044.
[22] B. Ma, X. Li, X. Shen, Y. Mao, H. Huang, Enhancing the addition of fly ash from thermal power plants in activated high belite sulfoaluminate cement, Constr. Build. Mater. 52 (2014) 261–266. doi:10.1016/j.conbuildmat.2013.10.099.
[23] T. Staněk, P. Sulovský, The influence of the alite polymorphism on the strength of the Portland cement, Cem. Concr. Res. 32 (2002) 1169–1175. doi:10.1016/S0008-8846(02)00756-1.
[24] R.B. Von Dreele, A.C. Larson, General structure analysis system (GSAS), Los Alamos Natl. Lab. Rep. LAUR. 748 (2004) 86–748.
[25] P. Thompson, D.E. Cox, J.B. Hastings, Rietveld Refinement of Debye-Scherrer Synchrotron X-ray Data from A1203, J. Appl. Crystallogr. 20 (1987) 79–83. doi:10.1107/S0021889887087090.
[26] L.W. Finger, D.E. Cox, A.P. Jephcoat, Correction for powder diffraction peak asymmetry due to axial divergence, J. Appl. Crystallogr. 27 (1994) 892–900. doi:10.1107/S0021889894004218.
[27] Á.G. De La Torre, S. Bruque, J. Campo, M.A.G. Aranda, The superstructure of C3S from synchrotron and neutron powder diffraction and its role in quantitative phase analyses, Cem. Concr. Res. 32 (2002) 1347–1356.
[28] A. Cuesta, E.R. Losilla, M.A.G. Aranda, J. Sanz, Á.G. De La Torre, Reactive belite stabilization mechanisms by boron-bearing dopants, Cem. Concr. Res. 42 (2012) 598–606.
[29] D.K. Smith, H.R. Leider, Low-temperature thermal expansion of LiH, MgO and CaO, J. Appl. Crystallogr. 1 (1968) 246–249. doi:10.1107/S0021889868005418.
[30] S. Sasaki, K. Fujino, Y. Takeuchi, X-ray determination of electron-density distributions in oxides, MgO, MnO, CoO, and NiO, and atomic scattering factors of their constituent atoms., Proc. Japan Acad. 55 (1979) 43–48.
[31] W.G. Mumme, R.J. Hill, G. Bushnell-Wye, E.R. Segnit, Rietveld crystal structure refinements, crystal chemistry and calculated powder diffraction data for the polymorphs of dicalcium silicate and related phases, Neues Jahrb. Fuer Mineral. 169 (1995) 35–68.
[32] A. Cuesta, A.G. De La Torre, E.R. Losilla, V.K. Peterson, P. Rejmak, A. Ayuela, C.

Frontera, M.A.G. Aranda, Structure, atomistic simulations, and phase transition of stoichiometric yeelimite, Chem. Mater. 25 (2013) 1680–1687. doi:10.1021/cm400129z.
[33] A. Cuesta, Á.G. De La Torre, E.R. Losilla, I. Santacruz, M.A.G. Aranda, Pseudocubic crystal structure and phase transition in doped ye'elimite, Cryst. Growth Des. 14 (2014) 5158–5163. doi:10.1021/cg501290q.
[34] A.A. Colville, S. Geller, The Crystal Structure of Brownmillerite, Ca2FeAlO5, Acta Cryst. 27 (1971) 5. doi:10.1107/S056774087100579X.
[35] P. Mondal, J.W. Jeffery, The crystal structure of tricalcium aluminate, Ca3Al2O6, Acta Crystallogr. Sect. B Struct. Crystallogr. Cryst. Chem. 31 (1975) 689–697. doi:10.1107/S0567740875003639.
[36] L. Palacios, A. Cabeza, S. Bruque, S. García-Granda, M.A.G. Aranda, Structure and electrons in mayenite electrides, Inorg. Chem. 47 (2008) 2661–2667. doi:10.1021/ic7021193.
[37] I. Pajares, A.G. De la Torre, S. Martínez-Ramírez, F. Puertas, M.-T. Blanco-Varela, M.A.G. Aranda, Quantitative analysis of mineralized white Portland clinkers: The structure of Fluorellestadite, Powder Diffr. 17 (2002). doi:10.1154/1.1505045.
[38] D. Speer, E. Salje, Phase transitions in langbeinites I: Crystal chemistry and structures of K-double sulfates of the langbeinite type M 2 + + K2(SO4)3, M + +=Mg, Ni, Co, Zn, Ca, Phys. Chem. Miner. 13 (1986) 17–24. doi:10.1007/BF00307309.
[39] A.G. De La Torre, S. Bruque, M.A.G. Aranda, Rietveld quantitative amorphous content analysis, J. Appl. Crystallogr. 34 (2001) 196–202. doi:10.1107/S0021889801002485.
[40] A.G. De la Torre, M.A.G. Aranda, Accuracy in Rietveld quantitative phase analysis of Portland cements, J. Appl. Crystallogr. 36 (2003). doi:10.1107/S002188980301375X.
[41] E. Tajuelo Rodriguez, K. Garbev, D. Merz, L. Black, I.G. Richardson, Thermal stability of C-S-H phases and applicability of Richardson and Groves' and Richardson C-(A)-S-H(I) models to synthetic C-S-H, Cem. Concr. Res. 93 (2017) 45–56. doi:10.1016/J.CEMCONRES.2016.12.005.
[42] G. Álvarez-Pinazo, I. Santacruz, L. León-Reina, M.A.G. Aranda, A.G. De La Torre, Hydration reactions and mechanical strength developments of iron-rich sulfobelite eco-cements, Ind. Eng. Chem. Res. 52 (2013) 16606–16614. doi:10.1021/ie402484e.
[43] G. Walenta, C. Comparet, V. Morin, E. Gartner, Hydraulic binder based on sulfoaluminate clinker and minerals additions., World Patent Application WO. 2010/070215 A1., 2010.
[44] G.S. Li, E. Gartner, High-belite sulfoaluminate clinker: fabrication process and binder preparation, French patent application 04-51586 (publication 2873366), 2006.
[45] D. Koumpouri, G.N. Angelopoulos, Effect of boron waste and boric acid addition on the production of low energy belite cement, Cem. Concr. Compos. 68 (2016) 1–8. doi:10.1016/j.cemconcomp.2015.12.009.
[46] M.T. Blanco-Varela, F. Puertas, T. Vázquez, A. Palomo, Modelling of the burnability of white cement raw mixes made with CaF2 and CaSO4, Cem. Concr. Res. 26 (1996) 457–464. doi:10.1016/S0008-8846(96)85033-2.
[47] Y. Zhao, L. Lu, S. Wang, C. Gong, Y. Huang, Modification of Dicalcium Silicates Phase Composition by BaO, SO3 and MgO, J. Inorg. Organomet. Polym. Mater. 23 (2013) 930–936. doi:10.1007/s10904-013-9873-2.
[48] D.H. Campbell, Microscopical Examination and Interpretation of Portland Cement and Clinker, Portland Cement Association, 1999.
[49] A. Gies, D. Knöfel, Influence of sulfur on the composition of belite-rich clinkers and the

technological properties of the resulting cements, Cem. Concr. Res. 17 (1987) 317–328. doi:10.1016/0008-8846(87)90114-1.
[50] J.M. Porras-Vázquez, A.G. De la Torre, E.R. Losilla, M.A.G. Aranda, Oxide and proton conductivity in aluminum-doped tricalcium oxy-silicate, Solid State Ionics. 178 (2007). doi:10.1016/j.ssi.2007.05.004.
[51] A. Cuesta, M.A.G. Aranda, J. Sanz, Á.G. De La Torre, E.R. Losilla, Mechanism of stabilization of dicalcium silicate solid solution with aluminium, Dalt. Trans. 43 (2014). doi:10.1039/c3dt52194j.
[52] T. Westphal, T. Füllmann, H. Pöllmann, Rietveld quantification of amorphous portions with an internal standard—Mathematical consequences of the experimental approach, Powder Diffr. 24 (2009) 239–243. doi:10.1154/1.3187828.
[53] A. Cuesta, J.D. Zea-Garcia, D. Londono-Zuluaga, A.G. De la Torre, I. Santacruz, O. Vallcorba, M. Dapiaggi, S.G. Sanfélix, M.A.G. Aranda, Multiscale understanding of tricalcium silicate hydration reactions, Sci. Rep. 8 (2018) 8544. doi:10.1038/s41598-018-26943-y.
[54] F. Winnefeld, S. Barlag, Influence of calcium sulfate and calcium hydroxide on the hydration of calcium sulfoaluminate clinker, ZKG Int. (2009) 42–53.
[55] A.J.M. Cuberos, A.G. De La Torre, G. Alvarez-Pinazo, M.C. Martín-Sedeño, K. Schollbach, H. Pöllmann, M.A.G. Aranda, Á.G. De La Torre, G. Álvarez-Pinazo, M.C. Martín-Sedeño, K. Schollbach, H. Pöllmann, M.A.G. Aranda, Active iron-rich belite sulfoaluminate cements: Clinkering and hydration, Environ. Sci. Technol. 44 (2010) 6855–6862.

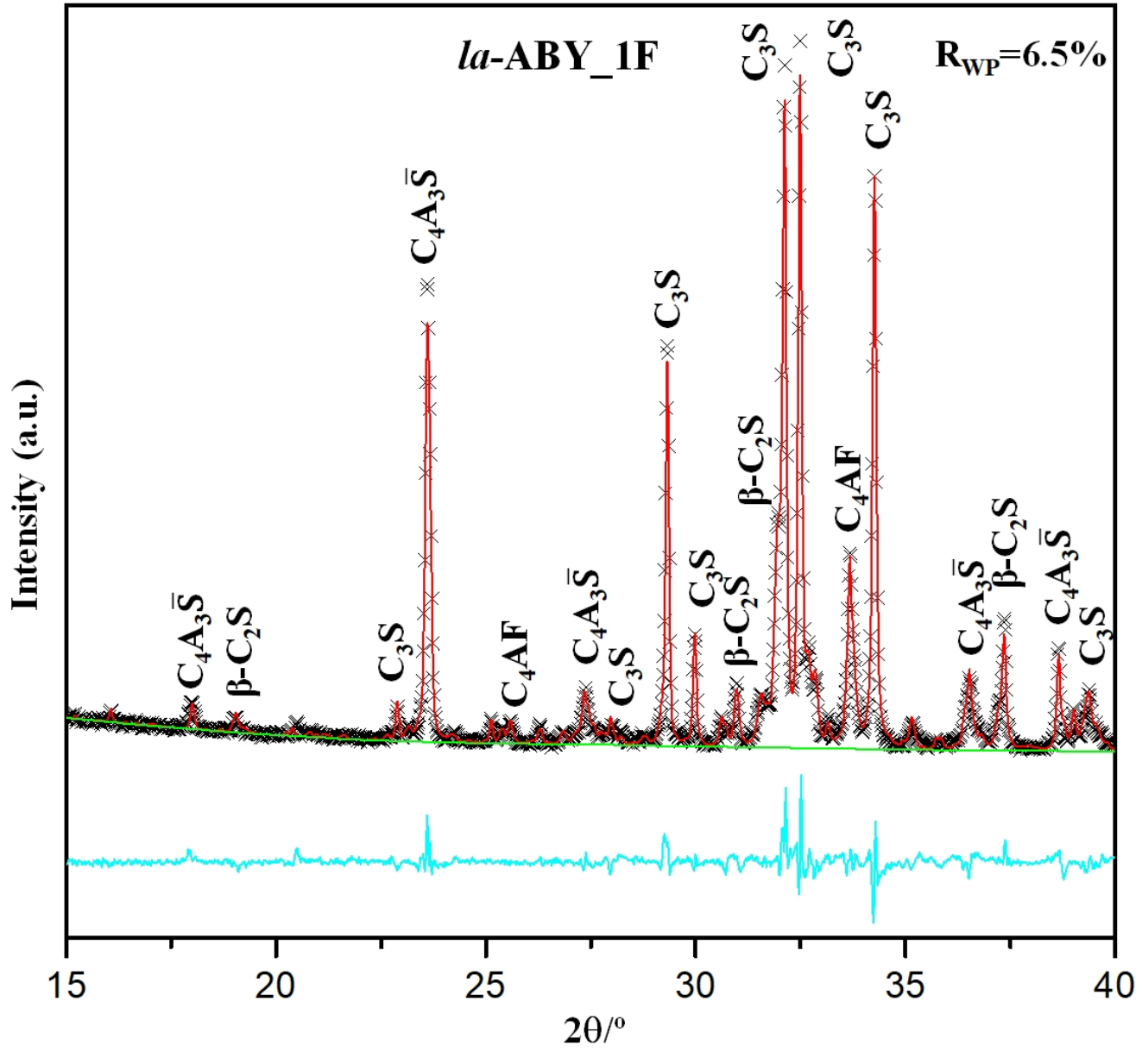
la-ABY_1F
R_WP=6.5%
Intensity (a.u.)
2θ/°
15
20
25
30
35
40
C4A3S̄
β-C2S
C3S
C4AF
C4A3S̄
C3S
C3S
β-C2S
C3S
C3S
C3S
C4AF
C4A3S̄
β-C2S
C4A3S̄
C3S

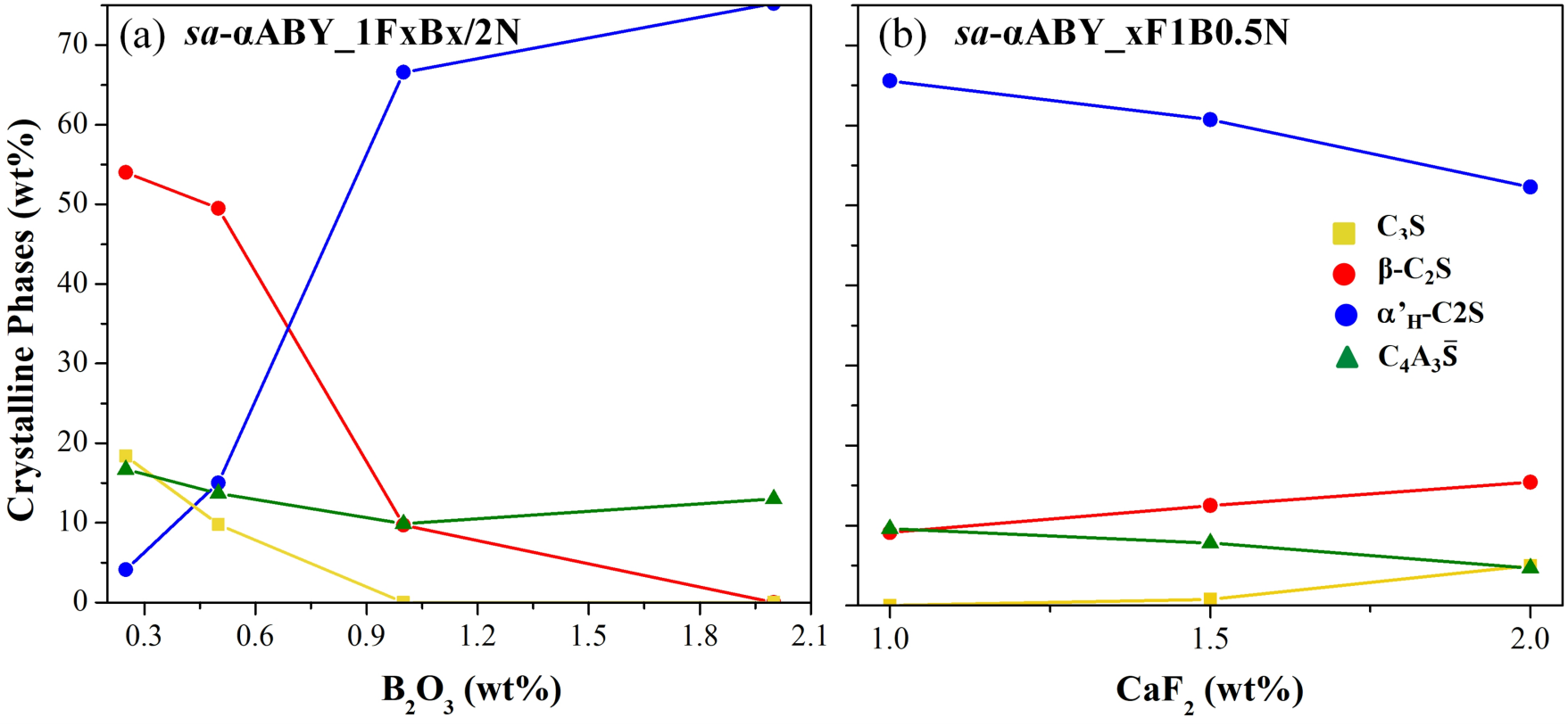
(a) sa-αABY_1FxBx/2N
(b) sa-αABY_xF1B0.5N
Crystalline Phases (wt%)
0
10
20
30
40
50
60
70
0.3
0.6
0.9
1.2
1.5
1.8
2.1
B2O3 (wt%)
1.0
1.5
2.0
CaF2 (wt%)
C3S
β-C2S
α'H-C2S
C4A3S̄

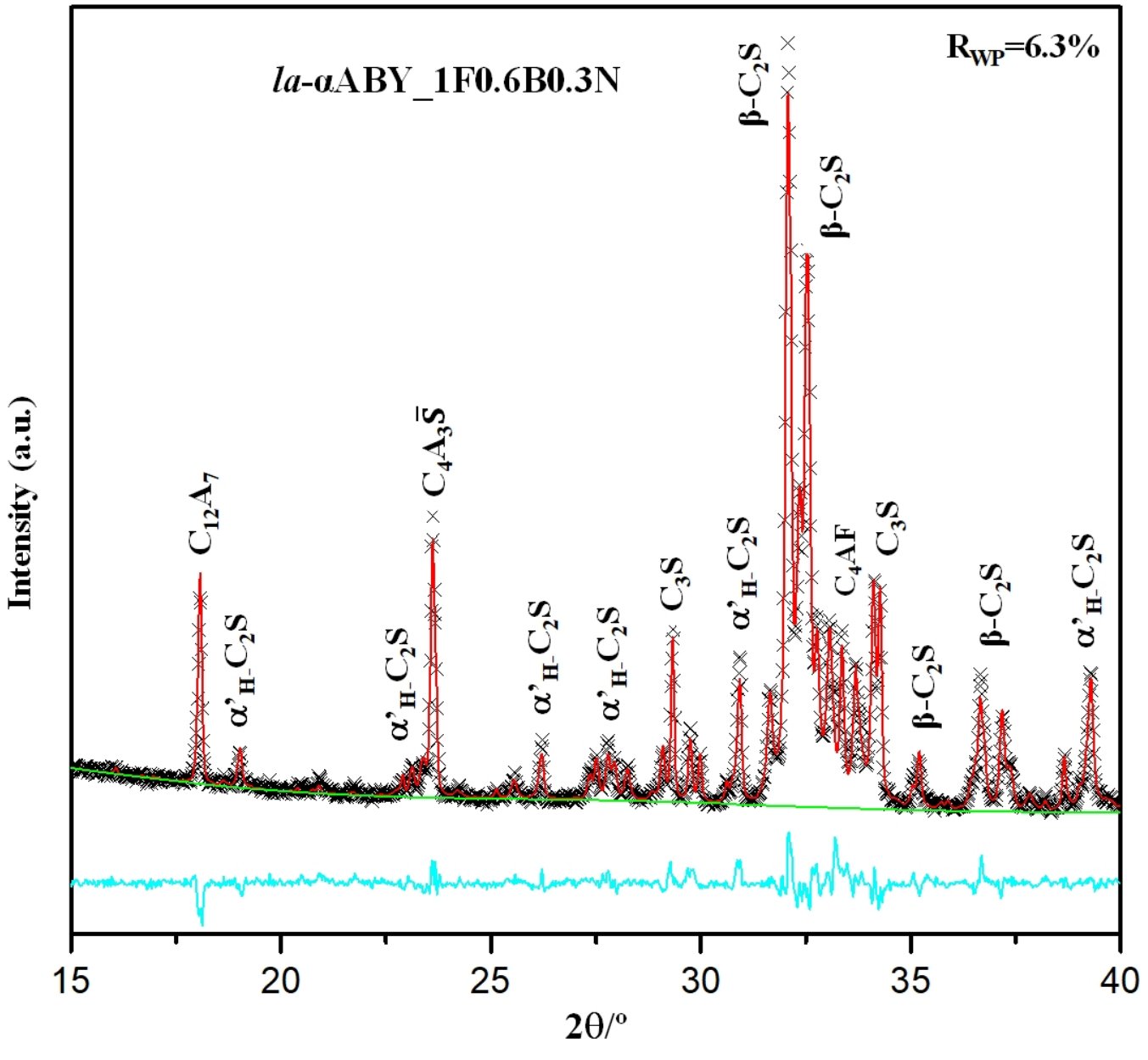
la-αABY_1F0.6B0.3N
R_WP=6.3%
Intensity (a.u.)
2θ/°
15
20
25
30
35
40
C12A7
α'H-C2S
α'H-C2S
C4A3S̄
α'H-C2S
α'H-C2S
C3S
α'H-C2S
β-C2S
β-C2S
C4AF
C3S
β-C2S
β-C2S
α'H-C2S

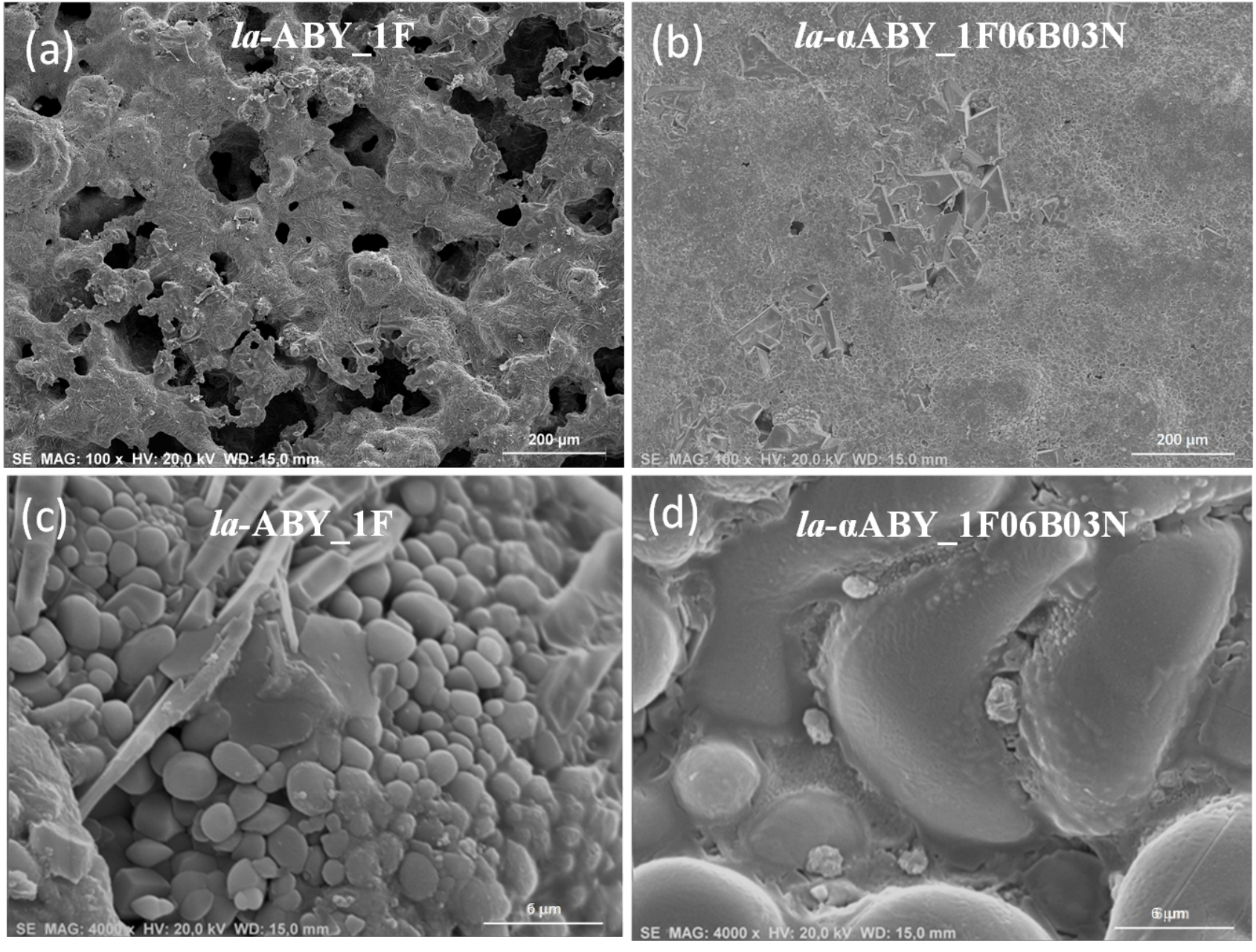
(a)
la-ABY_1F
200 µm
SE MAG: 100 x HV: 20,0 kV WD: 15,0 mm
(b)
la-αABY_1F06B03N
200 µm
SE MAG: 100 x HV: 20,0 kV WD: 15,0 mm
(c)
la-ABY_1F
6 µm
SE MAG: 4000 x HV: 20,0 kV WD: 15,0 mm
(d)
la-αABY_1F06B03N
6 µm
SE MAG: 4000 x HV: 20,0 kV WD: 15,0 mm

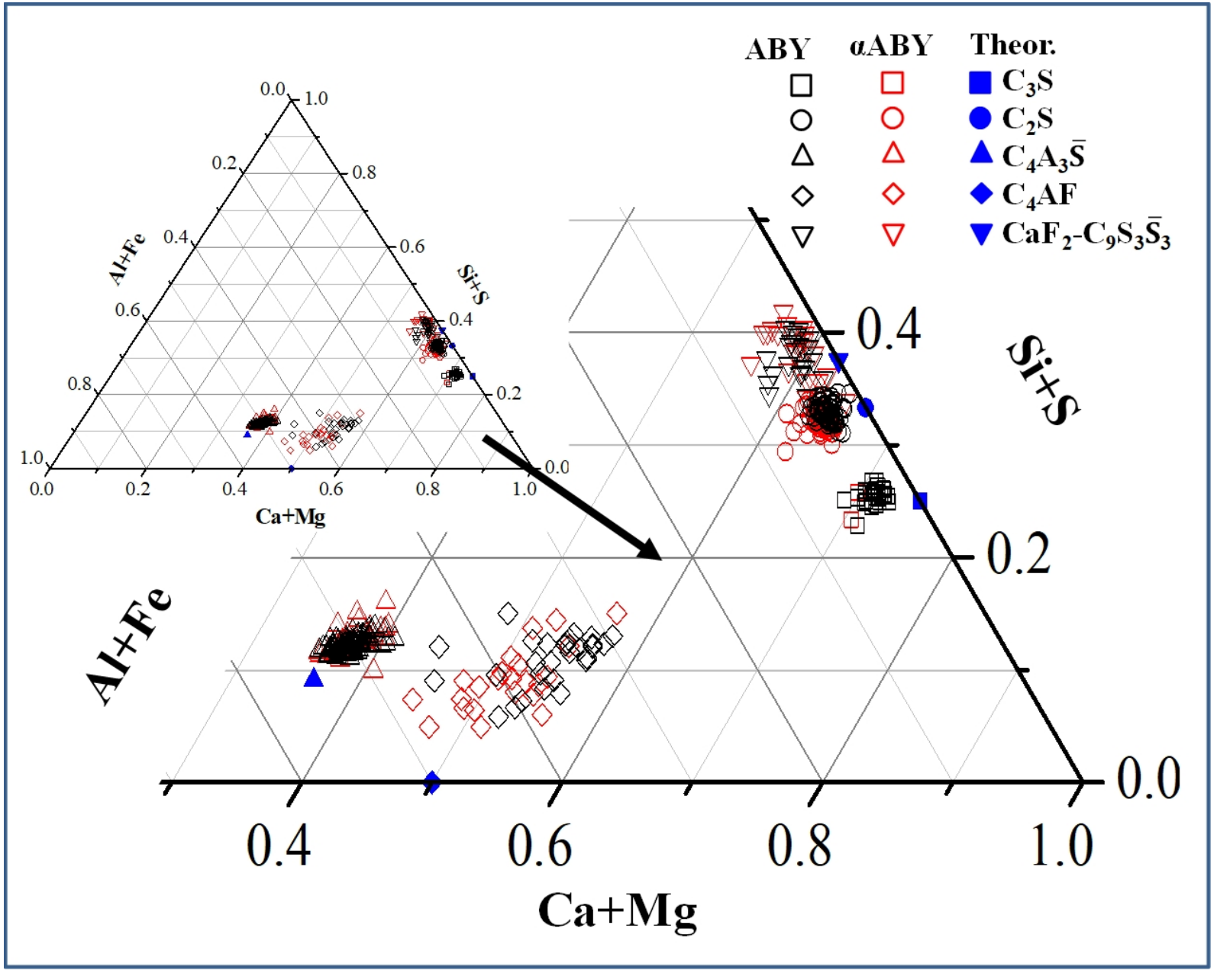
ABY
αABY
Theor.
C_3S
C_2S
$C_4A_3\bar{S}$
C_4AF
CaF_2-$C_9S_3\bar{S}_3$
Al+Fe
Si+S
Ca+Mg
0.0
0.2
0.4
0.6
0.8
1.0

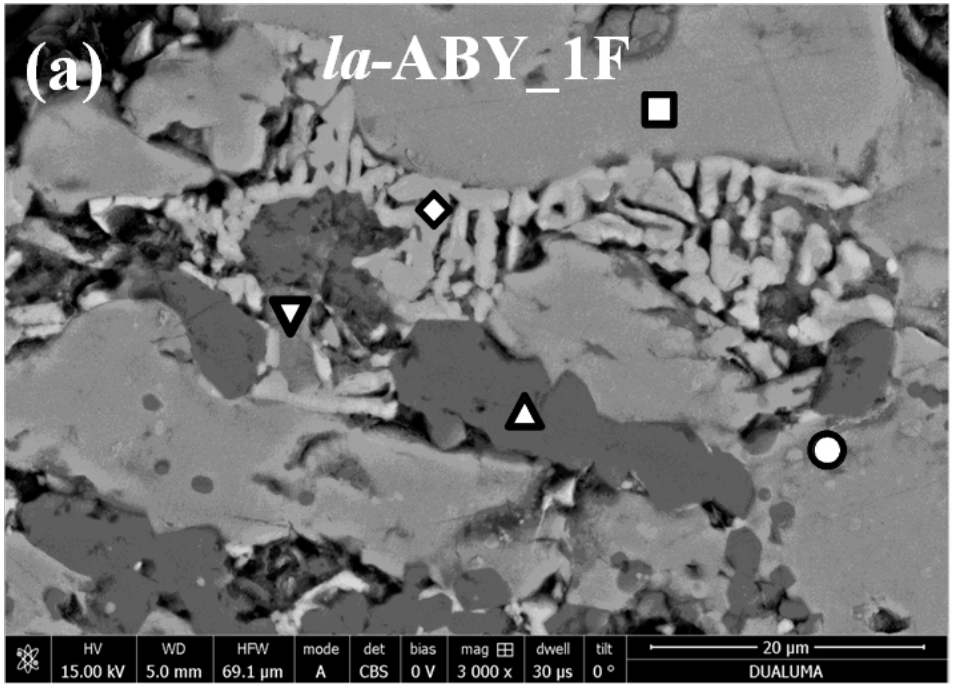
(a)
la-ABY_1F
HV
15.00 kV
WD
5.0 mm
HFW
69.1 µm
mode
A
det
CBS
bias
0 V
mag
3 000 x
dwell
30 µs
tilt
0 °
20 µm
DUALUMA

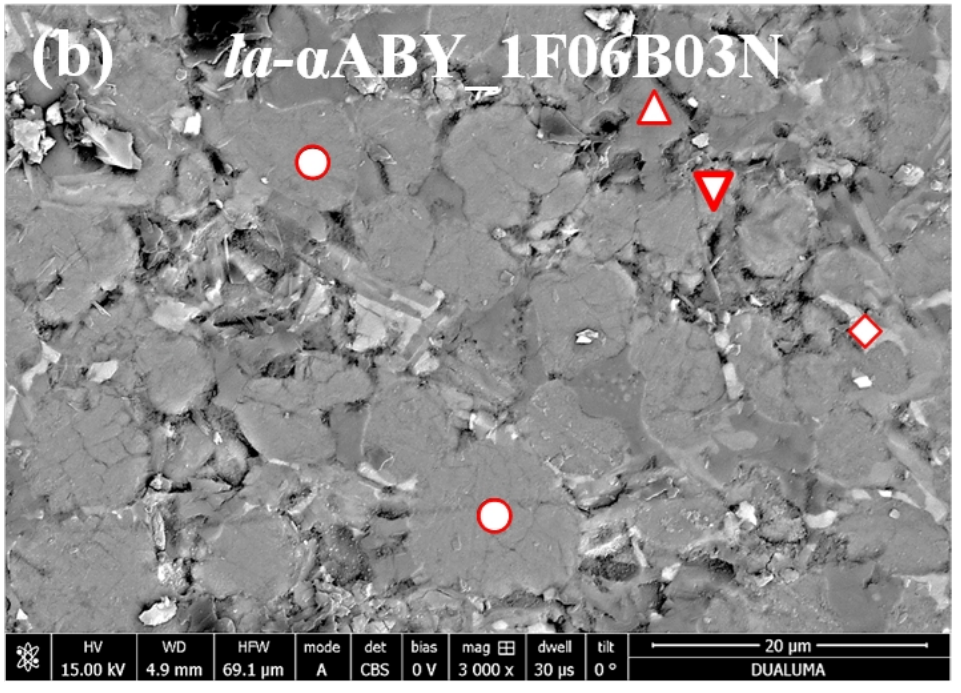
(b)
la-αABY_1F06B03N
HV
15.00 kV
WD
4.9 mm
HFW
69.1 µm
mode
A
det
CBS
bias
0 V
mag
3 000 x
dwell
30 µs
tilt
0 °
20 µm
DUALUMA

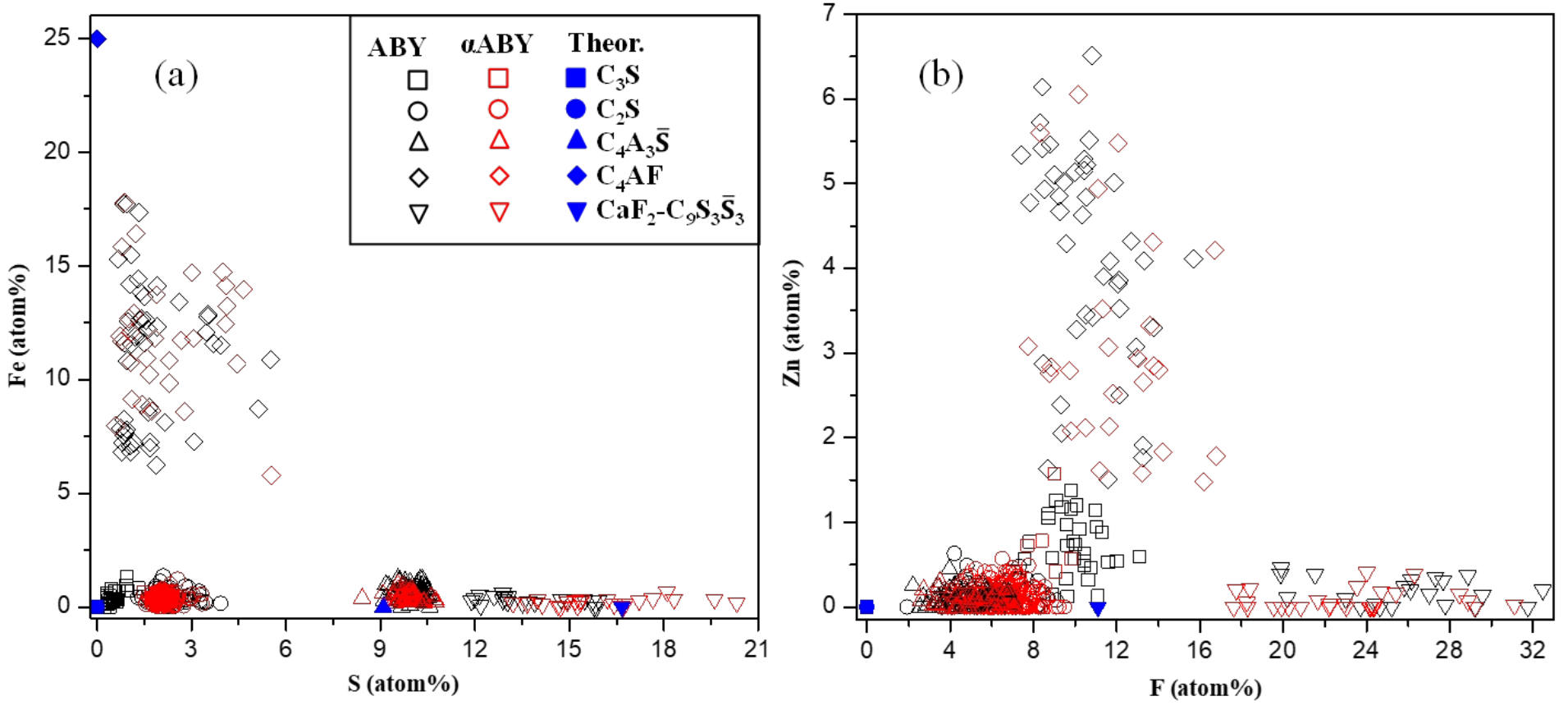
(a)
ABY
αABY
Theor.
C3S
C2S
C4A3S̄
C4AF
CaF2-C9S3S̄3
Fe (atom%)
S (atom%)
0
5
10
15
20
25
0
3
6
9
12
15
18
21
(b)
Zn (atom%)
F (atom%)
0
1
2
3
4
5
6
7
0
4
8
12
16
20
24
28
32

Compressive Strength

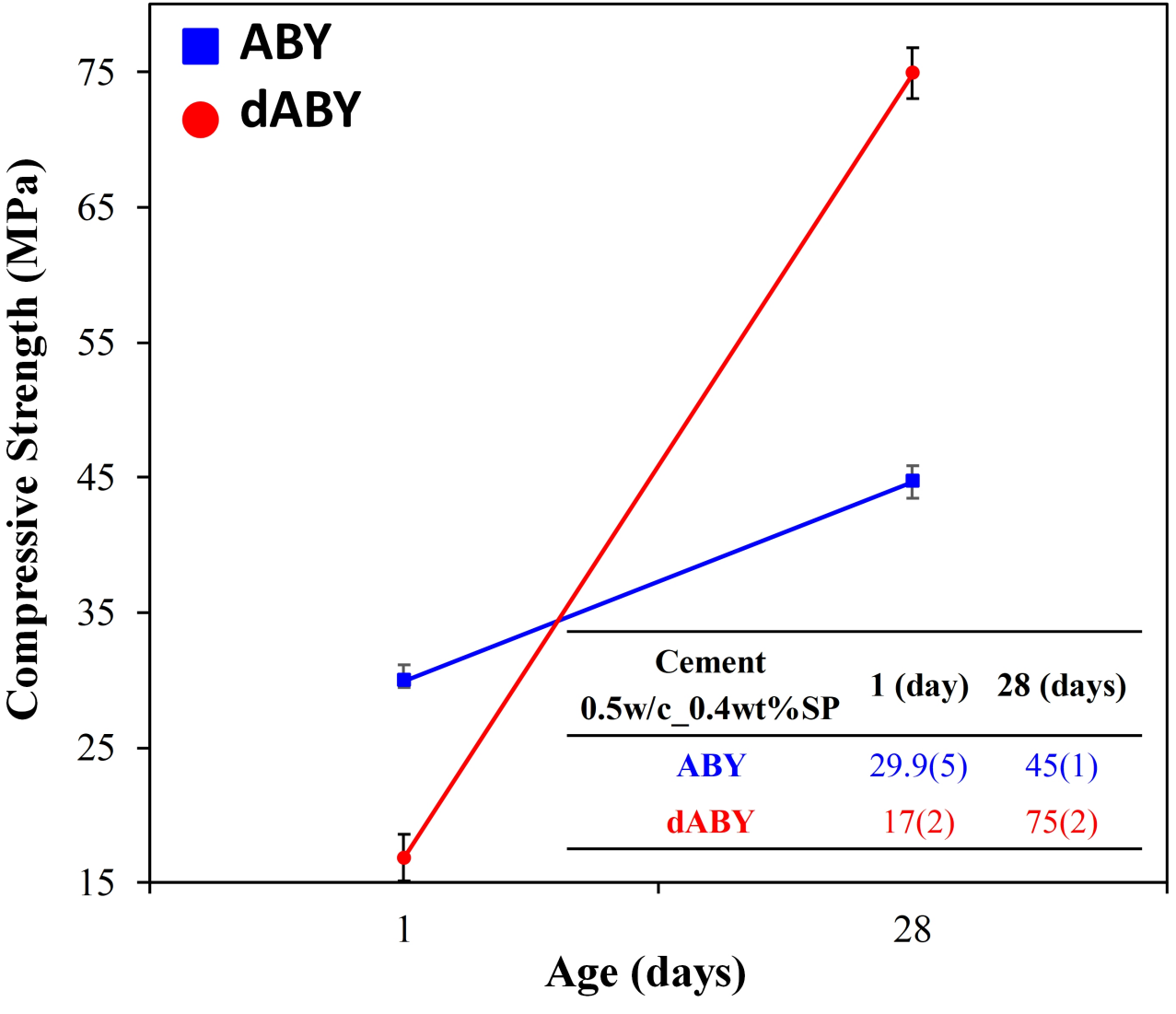

Cement 0.5w/c_0.4wt%SP	1 (day)	28 (days)
ABY	29.9(5)	45(1)
dABY	17(2)	75(2)

Supplementary information

Alite-Belite-Ye'elimite materials: effect of dopants on the clinker composition and properties

*Jesus D. Zea-Garcia[a], Isabel Santacruz[a], Miguel A.G. Aranda[a,b], Angeles G. De la Torre[a]**

[a] Departamento de Química Inorgánica, Cristalografía y Mineralogía, Universidad de Málaga, Málaga, 29071, Spain.

[b] ALBA Synchroton, Carrer de la Lum, 2-26, Cerdanyola, 08290, Barcelona-Spain.

* email: mgd@uma.es

This supplementary information includes Figures S1, S2 and S3 and Tables S1 and S2.

Raw XRPD patterns analyzed in the article can be found online on Zenodo at https://doi.org/10.5281/zenodo.1304464 and used under the Creative Commons Attribution license. The code of these files corresponds to the names of the samples analyzed in this article, where it is clearly explained what each one means. *.xrdml files have been collected with CuKα_1 monochromatic radiation and *.raw files with MoKα_1 monochromatic radiation.

aABY_0d.xrdml
aABY_1d.xrdml
aABY_28d.xrdml
ABY_0d.xrdml
ABY_1d.xrdml
ABY_28d.xrdml
la-aABY_1F06B03N.xrdml
la-aABY_1F06B03N_ACn.raw
la-ABY_1F.xrdml
la-ABY_1F_ACn.raw
ma-aABY_1F05B03N.xrdml
ma-aABY_1F06B03N.xrdml
ma-aABY_1F07B04N.xrdml

sa-aABY_15F1B05N.xrdml
sa-aABY_1F03B01N.xrdml
sa-aABY_1F05B03N.xrdml
sa-aABY_1F1B05N.xrdml
sa-aABY_1F1N.xrdml
sa-aABY_1F2B09N.xrdml
sa-aABY_1F2K.xrdml
sa-aABY_2F1B05N.xrdml

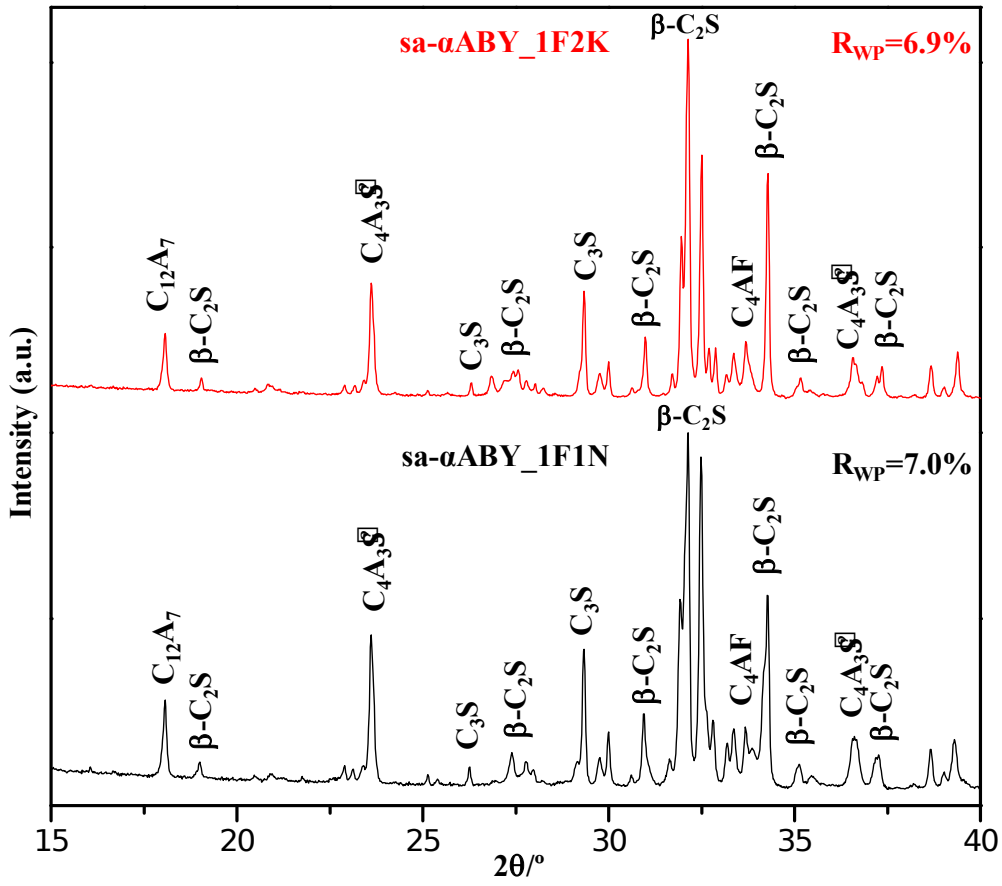

Figure S1. Raw LXRPD patterns of αABY_1F1N (bottom) and αABY_1F2K (top), with main peaks due to a given phase labeled.

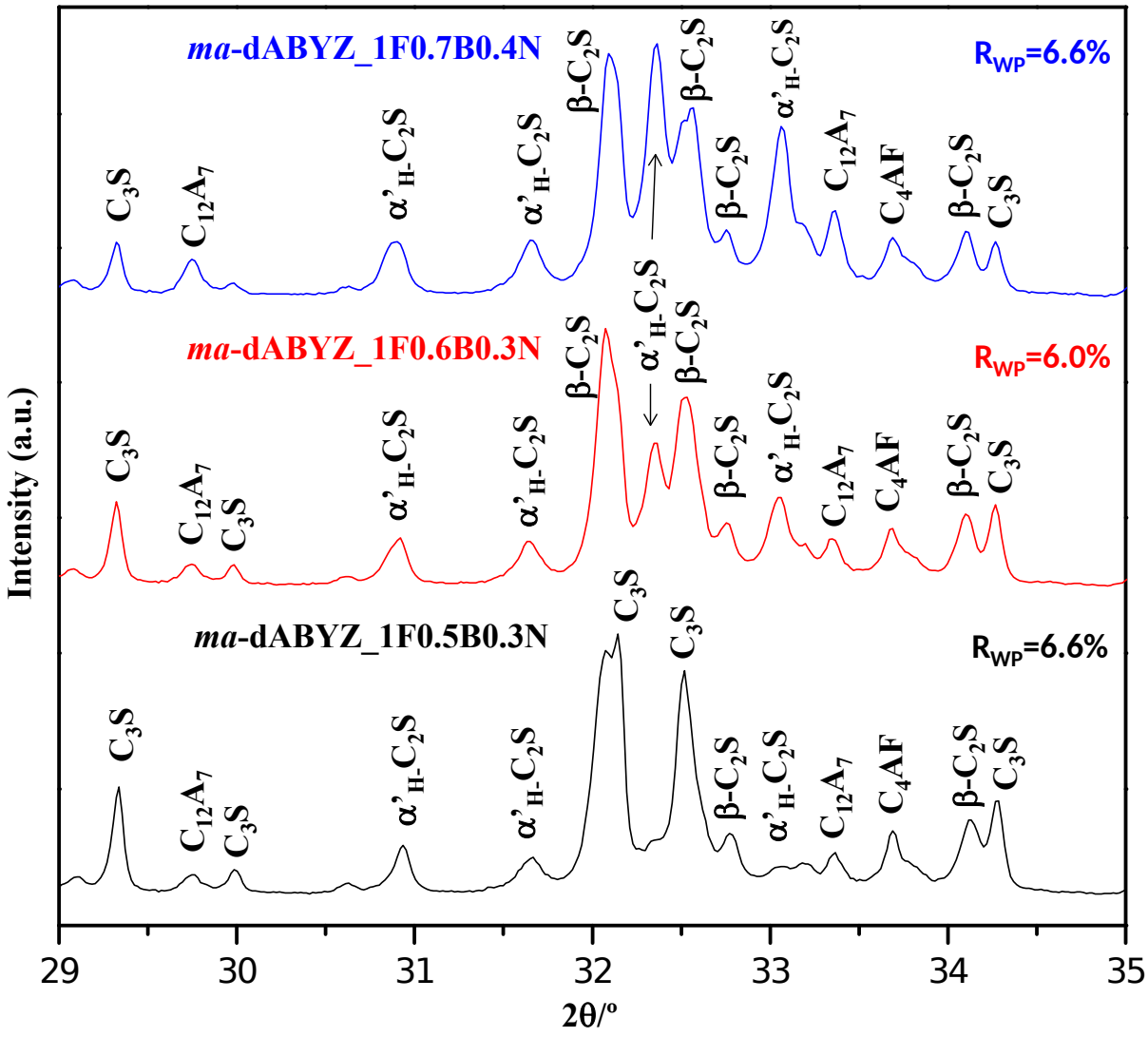

Figure S2. Raw LXRPD patterns of *ma*-αABY_1F0.5B0.2N (bottom), *ma*-αABY_1F0.6B0.3N (middle) and *ma*-αABY_1F0.8B0.3N (top), with main peaks due to a given phase labeled.

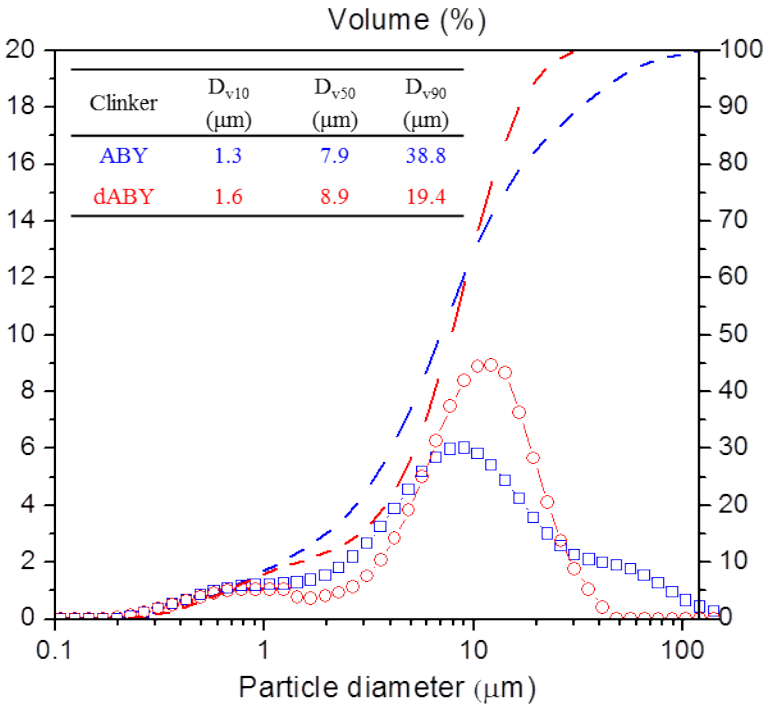

Figure S3. Particle size distribution of ABY and αABY powders after the preparation of 2 Kg each and milling. The inset shows the values of D_{v10}, D_{v50} and D_{v90}, of both samples.

Table S1. Elemental composition of raw materials expressed in weight percentage of oxides determined by XRF.

wt%	CaO	SiO_2	SO_3	Al_2O_3	Fe_2O_3	MgO	K_2O	Na_2O	ZnO	TiO_2	LoI*
Limestone	54.50(1)	1.00(1)	--	0.40(2)	0.10(1)	0.70(3)	--	--	--	--	43.10(1)
Gypsum	37.90(1)	8.00(1)	28.30(1)	2.80(1)	1.00(1)	2.10(1)	0.50(2)	0.20(2)	--	0.10(1)	18.80(1)
Kaolin	--	44.70(3)	--	38.90(1)	1.00(1)	0.30(1)	1.60(1)	0.20(2)	--	0.10(2)	13.00(1)
Sand	3.70(1)	83.30(1)	--	2.20(1)	1.80(1)	2.20(1)	0.30(1)	0.10(1)	--	0.10(1)	6.00(1)
Iron Ore	0.30(2)	8.50(1)	1.50(1)	1.20(1)	80.60(1)	0.30(2)	0.30(1)	0.60(5)	1.80(1)	0.10(1)	2.30(1)
Anhydrite	40.10(1)	1.00(1)	56.10(1)		0.10(3)	0.50(3)	0.03(2)	0.40(3)			1.31(3)

*LoI: Loss of Ignition

Table S2. Weight losses up to 600ºC (BW_{ATD}) for all the pastes *la*-ABY_1F and *la*-αABY_1F0.6B0.3N stopped pastes obtained from TGA curves.

***la*-ABY_1F**		*la*-αABY_1F0.6B0.3N	
1d / wt%	**28d / wt%**	**1d / wt%**	**28d / wt%**
22.0	28.1	17.7	30.1